Available online at www.sciencedirect.com
SCIENCE DIRECT®
Journal of Computational Physics 211 (2006) 659–699
JOURNAL OF COMPUTATIONAL PHYSICS
www.elsevier.com/locate/jcp

A class of difference schemes with flexible local approximation

Igor Tsukerman *

Department of Electrical and Computer Engineering, The University of Akron, Akron, OH 44325-3904, USA

Received 1 December 2004; received in revised form 17 April 2005; accepted 9 June 2005
Available online 10 August 2005

Abstract

Solutions of many physical problems have salient local features that are qualitatively known a priori (for example, singularities at point sources, edge and corners; boundary layers; derivative jumps at material interfaces; strong dipole field components near polarized spherical particles; cusps of electronic wavefunctions at the nuclei; electrostatic double layers around colloidal particles, etc.) The known methods capable of providing flexible local approximation of such features include the generalized finite element – partition of unity method, special variational-difference schemes in broken Sobolev spaces, and a few other specialized techniques. In the proposed new class of Flexible Local Approximation MEthods (FLAME), a desirable set of local approximating functions (such as cylindrical or spherical harmonics, plane waves, harmonic polynomials, etc.) defines a finite difference scheme on a chosen grid stencil. One motivation is to minimize the notorious 'staircase' effect at curved and slanted interface boundaries. However, the new approach has much broader applications. As illustrative examples, the paper presents arbitrarily high order 3-point schemes for the 1D Schrödinger equation and a 1D singular equation, schemes for electrostatic interactions of colloidal particles, electromagnetic wave propagation and scattering, plasmon resonances. Moreover, many classical finite difference schemes, including the Collatz "Mehrstellen" schemes, are direct particular cases of FLAME.

Keywords: Generalized finite difference method; Flexible approximation; Multiparticle problems; The Schrödinger equation; The Poisson–Boltzmann equation; Wave propagation; Scattering; Photonic crystals; Plasmon particles

1. Introduction: computational methods with flexible approximation

In many physical problems some salient features of the solution are qualitatively known a priori. Such features include singularities at point sources, edge and corners; boundary layers; derivative jumps at material interfaces; strong dipole field components near polarized spherical particles; cusps of electronic wavefunctions

* Tel.: +1 330 972 8041; fax: +1 330 972 6487.
E-mail address: igor@uakron.edu.

0021-9991/$ - see front matter © 2005 Elsevier Inc. All rights reserved.
doi:10.1016/j.jcp.2005.06.011

at the nuclei; electrostatic double layers around colloidal particles – and countless other examples. Such "special" behavior of physical fields is arguably a rule rather than an exception. Clearly, taking this behavior into account in numerical simulation will tend to produce more accurate and physically meaningful results.

The special features of the field are typically local, and in numerical modeling it is therefore desirable to employ various *local* approximations of the field. The focus of this paper is precisely on "flexible local approximation" and on methods capable of providing it – that is, employing a variety of approximating functions not at all limited to polynomials. It is from this angle that the existing approaches are reviewed (Section 2) and new ideas are considered. Section 4 introduces a new class of Flexible Local Approximation MEthods (FLAME), where the difference scheme is defined by the chosen set of local basis functions and the grid stencil.

One motivation for developing this class of methods is to minimize the notorious 'staircase' effect at curved and slanted interface boundaries on regular Cartesian grids. In the spirit of "flexible local approximation", the behavior of the solution at the interfaces is represented *algebraically*, by suitable basis functions on simple grids, rather than *geometrically* on conforming meshes. More specifically, fields around spherical particles can be approximated by several spherical harmonics; fields scattered from cylinders – by Bessel functions, and so on. Such analytical approximations are incorporated directly into the difference scheme.

This approach can be contrasted with very well known, and very powerful, finite element (FE) methodology, where the geometric features of the problem are represented on complex conforming meshes. The flexibility of approximation in FEM is achieved through adaptive mesh refinement: changing the mesh size (h-refinement) or the order of approximation (p-refinement). Still, approximation remains piecewise-polynomial; in fact, the polynomial space is an integral part of the standard definition of a finite element [22,17].

FEM is indispensable in many problems where the geometries are complex and material parameters vary. In addition to mechanical, thermal and electromagnetic modeling of traditional devices and machines, FEM has recently penetrated new areas of macromolecular simulation. Molecular interface surfaces can be viewed as intersections of hundreds or thousands of spheres and consequently are geometrically extremely complex. These interfaces separate the interior of the molecule, that can be approximated by an equivalent relative dielectric constant on the order of 1–4, from the solvent that in "implicit" models is considered as a continuum with equivalent dielectric and Debye parameters ([9,46,58,30,41,94,98] and references therein).

However, the computational overhead of mesh generation and matrix assembly in FEM is significant, and for geometrically simple problems FEM may not be competitive with finite difference (FD) schemes and other methods operating on simple Cartesian grids. One extreme example of geometric simplicity comes from molecular dynamics simulations, where charges or dipoles are typically considered in a cubic box with periodic boundary conditions. The Ewald algorithm (taking advantage of fast Fourier transforms) is then usually the method of choice.

Problems with multiple moving particles, such as for example in magnetically driven assembly [121,122], also call for development and application of new techniques. Generation of geometrically conforming FE meshes is obviously quite complicated or impractical when the particles move and their number is large (say, on the order of a hundred or more). Parallel adaptive generalized FEM has been developed [47–49], but the procedure is quite complicated both algorithmically and computationally. Standard FD schemes would require unreasonably fine meshes to resolve the shapes of all particles. An alternative approach is to use two types of grid: spherical meshes around the particles and a global Cartesian grid [44,36]. The electrostatic potential then has to be interpolated back and forth between the grids, which reduces the numerical accuracy.

The celebrated fast multipole method (FMM) has clear advantages for systems with a large number of known charges or dipoles in free space (or a homogeneous medium). For inhomogeneous media (e.g. a dielectric substrate, or finite size particles with dielectric or magnetic parameters different for those of free space) FMM can still be used as a fast matrix–vector multiplication algorithm imbedded in an iterative

process for the unknown distribution of volume sources. However, the benefits of FMM in this case are much less clear. An even stronger case in favor of difference schemes (as compared to FMM) can be made if the problem is nonlinear (for example, the Poisson–Boltzmann equation). FMM will remain outside the scope of this paper.

The proposed new FLAME schemes provide a practical alternative that is both uncomplicated and accurate (Section 4). In addition to multiparticle simulations, FLAME techniques can be applied to a variety of other problems. As a peculiar example, super high-order 3-point schemes are derived for the 1D Schrödinger equation in Sections 5.7, 5.8 and for a 1D singular equation in Section 5.9. With the 20th-order 3-point scheme as an illustration, the solution of the harmonic oscillator problem is found almost to machine precision with 10–20 grid nodes. The system matrix remains tridiagonal.

FLAME schemes are conceptually related to many other methods:

1. Generalized FEM by partition of unity [76,6,38,105,7,90,91,10] and "*hp*-cloud" methods [37].
2. Homogenization schemes based on variational principles [82].
3. Spectral and pseudospectral methods [16,35,86,87] (and references therein).
4. Meshless methods [12,11,29,32,66,70,7,69], and especially the "Meshless Local Petrov–Galerkin" version [4,3].
5. Heuristic homogenization schemes, particularly in finite difference time domain methods [34,106,124].
6. Discontinuous Galerkin (DG) methods [2,15,20,25,85].
7. Finite integration techniques (FIT) with extensions and enhancements [24,96].
8. Special FD schemes such as "exact" and "nonstandard" schemes by Mickens and others [78,79]; the Harari–Turkel [53] and Singer–Turkel schemes [99] for the Helmholtz equation; the Hadley schemes [50,51] for waveguide analysis; Cole schemes for wave propagation [26,27]; the Lambe–Luczak–Nehrbass schemes for the Helmholtz equation [68].
9. Special finite elements, for example elements with holes [101] or inclusions [73].
10. The "immersed surface" methodology [118] that modifies the Taylor expansions to account for derivative jumps at material boundaries but leads to rather unwieldy expressions.

This selection of related methods is to some extent subjective and definitely not exhaustive. Most methods and references above are included because they influenced the author's own research in a significant way; some references were suggested by the anonymous reviewers of this paper.

The connection of FLAME with methods 1–10, as well as the differences, are first highlighted in Section 2 and then revisited in Section 6. However, at the suggestion of the anonymous reviewer, a few points related to the nomenclature of the paper ought to be made immediately clear.

Even though the methods listed above (and reviewed in more detail in the following section) share some level of "flexible approximation" as one of their features, the term "Flexible Local Approximation MEthods" (FLAME) will in this paper refer exclusively to the approach developed in Sections 3 and 4. The new FLAME schemes are not intended to absorb or supplant any of the methods 1–10. These other methods, while related to FLAME, are not, generally speaking, its particular cases; nor is FLAME a particular case of any of these methods.

Consider, for example, a connection between FLAME on the one hand and variational homogenization (item 2 on the list above) and GFEM (item 1) on the other. The development of FLAME schemes was motivated to a large extent by the need to reduce the computational and algorithmic complexity of generalized FEM and variational homogenization (especially the volume quadratures inherent in these methods). However, FLAME is emphatically *not* a version of GFEM or variational homogenization of [82]. Indeed, GFEM is a Galerkin method in the functional space constructed by partition of unity; the variational homogenization is, as argued in [110], a Galerkin method in broken Sobolev spaces. In contrast, FLAME is in most cases a non-Galerkin, purely finite-difference method.

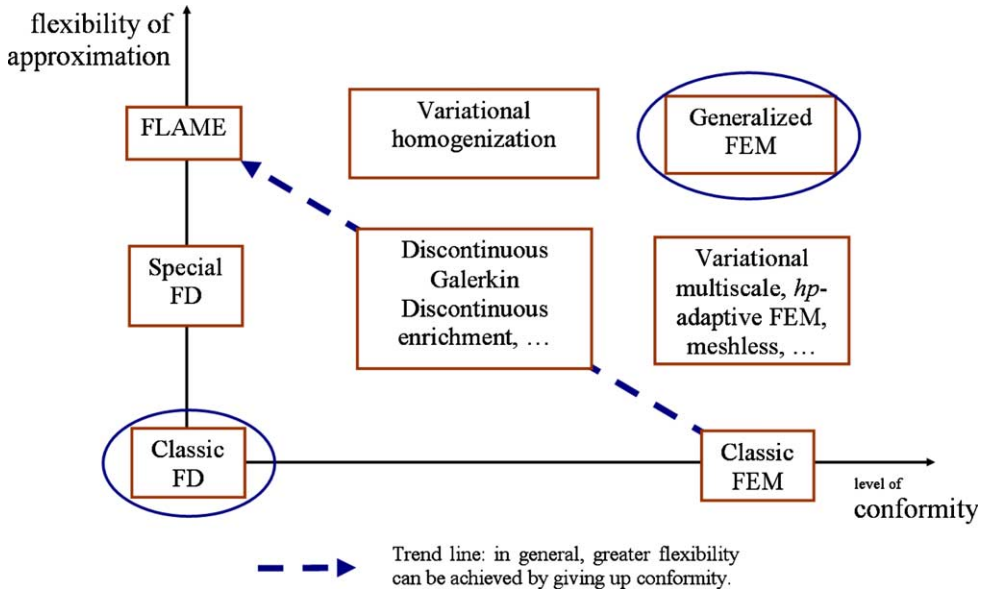

Fig. 1. A schematic "conformity vs. flexibility" view of various numerical methods. One can gain flexibility of approximation by giving up conformity. This general trend is indicated by the dashed arrow. GFEM *outperforms* this trend, at a high computational and algorithmic cost. Classic FD schemes *underperform*. FLAME schemes fill the existing void.

The following very schematic chart (Fig. 1) puts various methods into a "flexibility vs. conformity" perspective. As a general trend, flexibility of approximation can be gained by giving up some conformity of the method. Two methods stand out of that trend: GFEM and classic FD.

GFEM *outperforms* the trend: it is fully conforming (i.e. operating in a globally defined subspace of the relevant Sobolev space) and yet allows any desirable approximating functions to be used. However, this advantage is achieved at a high computational and algorithmic cost. Classic FD schemes *under*perform relative to the general trend: they are fully nonconforming and yet make use only of local polynomial (i.e. Taylor) expansions.

FLAME schemes fill the existing void in the upper-left corner of the chart: they are fully nonconforming[1] and admit arbitrary approximations.

Clearly, it would be somewhat simplistic to ask which side of this chart is "better". No one would question the tremendous success of conventional FE analysis lying at the 'conformal' end. However, the conformity requirements do impose significant limitations in many practical cases. This was understood early on in the development of FEM – hence the notion of 'variational crimes' [103,17], the Crouzeix–Raviart elements [31], the discontinuous Galerkin methods, variational homogenization [82], etc. The advantages of the *non*conforming end of the spectrum are particularly clear for problems with multiple moving particles, where finite element mesh generation may be inefficient or impractical.

The FLAME schemes have undergone several stages of development. As mentioned earlier, the generalized FEM and variational homogenization served as a starting point for this research. The variational version of FLAME then followed and was described in [109] in a condensed manner. Section 3.3 of the present paper incorporates this description to provide the necessary background and to make this paper self-contained. In particular, the framework of "multivalued approximation" introduced in Section 3.3 will

[1] It is argued in Section 3.3 that "multivalued approximation" is the proper framework for treating these methods.

be needed in subsequent sections. Proofs of consistency and (under the assumption of monotonicity) convergence of variational FLAME are also given.

The crux of this paper, however, is the nonvariational 'Trefftz' version of FLAME (Section 4). In this version, the basis functions satisfy the underlying differential equation and the variational testing is therefore redundant. Numerical quadratures – the main bottleneck of generalized FEM, variational homogenization, meshless and other methods – are completely absent. Despite their relative simplicity, the Trefftz-FLAME schemes are in many cases more accurate than their variational counterparts.

Section 5 presents a variety of examples for Trefftz-FLAME, including the 1D Schrödinger equation, a singular 1D equation, 2D and 3D Collatz "Mehrstellen" schemes, and others. The complementary paper [111] provides a variety of *electromagnetic* applications of FLAME: electrostatic many-body interactions with and without solvents; electromagnetic wave propagation in photonic crystals; scattering of electromagnetic waves from dielectric particles. For completeness, these applications are briefly reviewed here in Section 5.10. An interesting new electromagnetic example of Trefftz-FLAME is given in Section 5.11. It involves plasmon resonances of two coupled cylindrical nanoparticles in close proximity to one another.

The novelty of the present paper is in providing a mathematical description and background for Trefftz-FLAME difference schemes (including proofs of consistency and convergence) and in extending these new schemes beyond electromagnetic applications. Methodologically, the main new feature is the systematic use of local approximation spaces *in the FD context*. It is hoped that the proposed framework, with its extensive connections to many existing approaches, will stimulate further development of finite difference and finite element methods.

2. An overview of existing methods featuring flexible or nonstandard approximation

2.1. Treatment of singularities in standard FEM

The treatment of singularities was historically one of the first cases where special approximating functions were used in the FE context. In their 1973 paper [40], Fix, Gulati and Wakoff considered 2D problems with singularities $r^\gamma \sin \beta\phi$, where r, ϕ are the polar coordinates with respect to the singularity point, and β, γ, are known parameters ($\gamma < 0$). The standard FEM bases were enriched with functions of the form $p(r)r^\gamma \sin \beta\phi$, where the piecewise-polynomial cutoff function $p(r)$ is unity within a disk $0 \leqslant r \leqslant r_0$, gradually decays to zero in the ring $r_0 \leqslant r \leqslant r_1$ and is zero outside that ring (r_0 and r_1 are adjustable parameters). The cutoff function is needed to maintain the sparsity of the stiffness matrix.

There is clearly a tradeoff between the computational cost and accuracy: if the cutoff radius r_1 is too small, the singular component of the solution is not adequately represented; but if it is too large, the support of the additional basis function overlaps with a large number of elements and the matrix becomes less sparse.

The generalized FEM (GFEM) briefly described in the following subsection preserves, at least in principle, both accuracy and sparsity. Unfortunately, this major advantage is tainted by additional algorithmic and computational complexity.

2.2. Generalized FEM by partition of unity

In the generalized FEM [76,6,38,105,7], computational domain Ω is covered by overlapping subdomains ('patches') $\Omega^{(i)}$. Our notational convention is to reserve the *super*script for the patch number and to use *sub*scripts for the individual approximating functions within each patch. The solution is approximated locally over each patch. These individual local approximations are independent from one another and are merged by partition of unity (PU).

More precisely, a set of PU functions $\{\varphi^{(i)}\}$, $1 \leqslant i \leqslant n_{\text{patches}}$ is constructed on this system of patches to satisfy

$$\sum_{i=1}^{n_{\text{patches}}} \varphi^{(i)} \equiv 1 \quad \text{in } \Omega, \quad \operatorname{supp} \varphi^{(i)} = \Omega^{(i)}. \tag{1}$$

That is, each function $\varphi^{(i)}$ is associated with the respective patch $\Omega^{(i)}$ and vanishes outside that patch. Then the global solution u can be decomposed into its 'patch components' $u^{(i)}$

$$u = u \sum_{i=1}^{n_{\text{patches}}} \varphi^{(i)} = \sum_{i=1}^{n_{\text{patches}}} u\varphi^{(i)} = \sum_{i=1}^{n_{\text{patches}}} u^{(i)} \quad \text{with } u^{(i)} \equiv u\varphi^{(i)}. \tag{2}$$

Fig. 2 gives a simple 1D illustration of the PU principle, with just two overlapping patches. A seamless transition from the solution in the first patch to the solution in the second patch is achieved by multiplying these individual solutions by the weighting functions $\varphi^{(1)}$ and $\varphi^{(2)}$, respectively. As a reference point moves from left to right, the weight of the first solution gradually decreases, while simultaneously the weight of the second solution increases.

Decomposition (2) is valid for the exact solution but can equally well be used for assembling the global *approximate* solution from the local ones. Suppose that locally, within each patch $\Omega^{(i)}$, the exact solution u can be approximated by a linear combination $u_h^{(i)}$ of some approximating functions $g_\alpha^{(i)}$:

$$u_h^{(i)} = \sum_\alpha c_\alpha^{(i)} g_\alpha^{(i)}. \tag{3}$$

The final system of approximating functions $\psi_\alpha^{(i)}$ is built with $\varphi^{(i)}$ as weight functions:

$$\psi_\alpha^{(i)} = g_\alpha^{(i)} \varphi^{(i)}. \tag{4}$$

The global approximation error is guaranteed to be bounded by the local (patch-wise) errors [6,105,7], with rigorously provable estimates of the global error in terms of local errors and the norms of the PU functions ϕ. A detailed explanation and analysis of this method proposed originally by Babuška and Melenk is widely available. For example, Strouboulis et al. [105] present an extensive set of application examples with special functions for material inclusions in stress analysis. Babuška et al. [5] apply GFEM (still at the early stages of development in 1994) to problems with material interfaces. Plaks et al. [90] implemented GFEM for problems with magnetized particles.

The main advantage of GFEM is that the approximating functions can in principle be arbitrary and are certainly not limited to polynomials. Thus GFEM definitely qualifies as a method with the kind of flexible local approximation we seek.

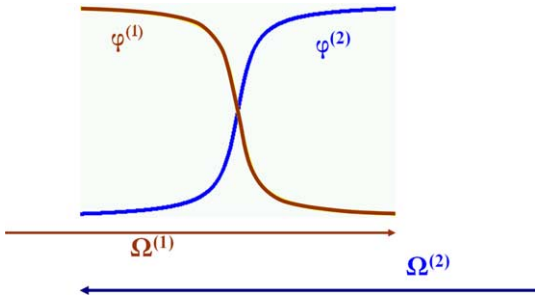

Fig. 2. The idea of partition of unity illustrated in 1D: weighting functions $\varphi^{(1)}$ and $\varphi^{(2)}$ used to merge two solutions in the overlapping subdomains. The sum of the weighting functions is unity everywhere.

On the negative side, however, multiplication by the partition of unity functions makes the system of approximating functions more complicated, and possibly ill-conditioned or even linearly dependent [6]. The computation of gradients and implementation of the Dirichlet conditions also get more complicated. In addition, GFEM-PU may lead to a combinatorial increase in the number of degrees of freedom [90,110]. An even greater difficulty in GFEM-PU is the high cost of the Galerkin quadratures that need to be computed numerically in geometrically complex 3D regions (intersections of overlapping patches).

In summary, there is a high algorithmic and computational price to be paid for all the flexibility that GFEM provides.

2.3. Homogenization schemes based on variational principles

Moskow et al. [82] improve the approximation of the electrostatic potential near slanted boundaries and narrow sheets on regular Cartesian grids by employing special approximating functions constructed by a coordinate mapping [5]. Within each grid cell, the authors seek a tensor representation of the material parameter such that the discrete and continuous energy inner products are the same over the chosen discrete space. The overall construction in [82] relies on a special partitioning of the grid (''red–black'' numbering, or the ''Lebedev grid'') and on a specific, central difference, representation of the gradient. As shown in [110], this variational homogenization can be interpreted as a Galerkin method in a broken Sobolev space.

The variational method described in Section 3 can be viewed as an extension of the variational-difference approach of [82] – the special 'Lebedev' grids and the specific approximation of gradients by central differences adopted in [82] turn out not to be really essential for the algorithm.

2.4. Discontinuous Galerkin methods

The idea to relax the interelement continuity requirements of the standard FEM and to use nonconforming elements was put forward at the early stages of FE research. For example, in the Crouzeix–Raviart elements [31] the continuity of piecewise-linear functions is imposed only at midpoints of the edges.

Over recent years, a substantial amount of work has been devoted to discontinuous Galerkin methods (DGM) [15,20,25,85]; a consolidated view with extensive bibliography is presented in [2]. Many of the approaches start with the ''mixed'' formulation that includes additional unknown functions for the fluxes on element edges (2D) or faces (3D). However, these additional unknowns can be replaced with their numerical approximations, thereby producing a ''primal'' variational formulation in terms of the scalar potential alone. In DGM, the interelement continuity is ensured, at least in the weak sense, by retaining the surface integrals of the jumps, generally leading to saddle-point problems even if the original equation is elliptic.

2.5. Homogenization schemes in FDTD

Finite difference time domain (FDTD) methods of applied electromagnetics require very extensive computational work due to a large number of time steps for numerical wave propagation and large meshes. Therefore simple Cartesian grids are strongly preferred and the need to avoid 'staircase' approximations of curved or slanted boundaries is quite acute. Due to the wave nature of the problem, any local numerical error, including the errors due to the staircase effect, tend to propagate in space and time and pollute the solution overall.

A great variety of approaches to reduce or eliminate the staircase effect in FDTD have been proposed [34,106,124,125]. Each case is a trade-off between the simplicity of the original Yee scheme on staggered grids [119] and the ability to represent the interface boundary conditions accurately. On one side of this spectrum lie various adjustments to the Yee scheme: changes in the time-stepping formulas for the magnetic field or heuristic homogenization of material parameters based on volume or edge length ratios [34,106,124]. In some cases, the second order of the FDTD scheme is maintained by including additional

geometric parameters or by using partially filled cells, as done by Zagorodnov et al. [125] in the framework of "finite integration techniques".

On the other side of the spectrum are finite volume – time domain methods (FVTD) [89,106,120] with their historic origin in computational fluid mechanics, and the finite element method (FEM). Tetrahedral meshes are typically used, and material interfaces are represented much more accurately than on Cartesian grids. (However, adaptive Cartesian grids have also been advocated, with cell refinement at the boundaries [115].) The greater geometric flexibility of these methods is achieved at the expense of simplicity of the algorithm. FEM has an additional disadvantage for time-domain problems: the "mass" matrix (containing the inner products of the basis functions) appears in the time derivative term and makes the time-stepping procedure implicit, unless "mass-lumping" techniques are used.

2.6. Meshless methods

The abundance of meshless methods, as well as many variations in the terminology adopted in the literature, make a thorough review unfeasible here – see [12,11,29,32,66,70,7] instead. We only highlight the main ideas and features.

The prevailing technique is the moving least squares (MLS) approximation. Consider a 'meshless' set of nodes (that is, nodes selected at arbitrary positions r_i, $i = 1, 2, \ldots, n$) in the computational domain. For each node i, a smooth weighting function $W_i(r)$ with a compact support is introduced; this function would typically be normalized to one at node i (i.e. at $r = r_i$) and decay to zero away from that node. Intuitively, the support of the weighting function defines the "zone of influence" for each node.

Let u be a smooth function that we wish to approximate by MLS. For any given point r_0, one considers a linear combination of a given set of m basis functions $\psi_\alpha(r)$ (almost always polynomials in the MLS framework): $u_h^{(i)} = \sum_{\alpha=1}^{m} c_\alpha(r_0)\psi_\alpha(r)$. Note that the coefficients c depend on r_0. They are chosen to approximate the nodal values of u, i.e. the Euclidean vector $\{u(r_i)\}$, in the least-squares sense with respect to the weighted norm with the weights $W_i(r_0)$. This least-squares problem can be solved in a standard fashion; note that it involves only nodes containing r_0 within their respective "zones of influence" – in other words, only nodes i for which $W_i(r_0) \neq 0$.

Duarte and Oden [37] showed that this procedure can be recast as a partition of unity method, where the PU functions are defined by the weighting functions W as well as the (polynomial) basis set $\{\psi\}$. This leads to more general adaptive "*hp*-cloud" methods.

One version of meshless methods – "meshless local Petrov–Galerkin" (MLPG) method developed by Atluri et al. [4,3,69] – is particularly close to the variational version of FLAME described in [109] and in Section 3 below. Our emphasis, however, is not on the 'meshless' setup (even though it is conceivable for FLAME) but on the framework of multivalued approximation (that is not explicitly introduced in MLPG) and on the new *non*variational version of FLAME (Section 4).

The trade-off for avoiding complex mesh generation in mesh-free methods is the increased computational and algorithmic complexity. The expressions for the approximating functions obtained by least squares are rather complicated [11,32,66,70,7]. The *derivatives* of these functions are even more involved. These derivatives are part of the integrand in the Galerkin inner product, and the computation of numerical quadratures is a bottleneck in meshless methods. Other difficulties include the treatment of Dirichlet conditions and interface conditions across material boundaries [29,32,66,70].

2.7. Pseudospectral methods

In pseudospectral methods (PSM) [16], numerical solution is sought as a series expansion in terms of Fourier harmonics, Chebyshev polynomials, etc. The expansion coefficients are found by collocating the differential equation on a chosen set of grid nodes.

Typically the series is treated as *global* – over the whole domain or large subdomains. There are, however, many versions of pseudospectral methods, some of which (''spectral elements'') deal with more localized approximations and in fact overlap with the *hp*-version of FEM [77].

The key advantage of PSM is their exponential convergence, provided that the solution is quite smooth over the whole domain.

One major difficulty is the treatment of complex geometries. In relatively simple cases this can be accomplished by a global mapping to a reference shape (square in 2D or cube in 3D) but in general may not be possible. Another alternative is to subdivide the domain and use spectral elements (with 'spectral' approximation within the elements but lower order smoothness across their boundaries); however, convergence is then algebraic, not exponential, with respect to the parameter of that subdivision.

The presence of material interfaces is an even more serious problem, as the solution then is no longer smooth enough to yield the exponential convergence of the global series expansion.

An additional disadvantage of PSM is that the resultant systems of equations tend to have much higher condition numbers than the respective FD or FE systems [83]. This is due to the very uneven spacing of the Chebyshev or Legendre collocation nodes typically used in PSM. Ill-conditioning may lead to accuracy loss in general and to stability problems in time-stepping procedures.

PSM have been very extensively studied over the last 30 years, and quite a number of approaches alleviating the above disadvantages have been proposed [35,77,83,86]. Nevertheless it would be fair to say that these disadvantages are inherent in the method and impede its application to problems with complex geometries and material interfaces.

Pseudospectral methods could technically be considered as a particular case of the *variational* version of FLAME schemes in Section 3, if the basis set is chosen as Fourier harmonics or Chebyshev polynomials, etc., and the test functionals are the Dirac deltas. However, the emphasis in FLAME is on *local* approximation, precisely to capture behavior of the solution that cannot be easily treated by global spectral expansions (e.g. discontinuities at material interfaces).

2.8. Special difference schemes

Many difference schemes rely on special approximation techniques to improve the numerical accuracy. These special techniques are too numerous to list, and only the ones that are more closely related to the ideas of this paper are briefly reviewed below.[2]

For 1D equations with constant coefficients, ''exact'' FD schemes – that is, schemes with zero consistency error – are fairly well known (see e.g. [88,78]). These ''exact'' schemes happen to be a direct particular case of the Trefftz-FLAME methods introduced in Section 4. Mickens also developed a wider class of ''nonstandard'' schemes by modifying finite difference approximations of derivatives. These modified approximations are *asymptotically* (as the mesh size tends to zero) equivalent to the standard ones but for finite mesh sizes may yield higher accuracy. Similar ideas were used by Harari and Turkel [53] and Singer and Turkel [99] to construct exact and high-order schemes for the Helmholtz equation in 1D, 2D and 3D. Cole [26,27] has applied nonstandard methods to electromagnetic wave propagation problems (high-order schemes) in 2D and 3D.

Nehrbass [84] and Lambe et al. [68] modified the central coefficient of the standard FD scheme for the Helmholtz equation to minimize, in some sense, the average consistency error over plane waves propagating in all possible directions. Some similarity between the Nehrbass schemes and FLAME will become obvious in Section 4. However, the derivation of the Nehrbass schemes requires very elaborate symbolic

[2] I would like to thank the anonymous reviewers of this paper for pointing out additional methods and references.

algebra coding, as the averaging over all directions of propagation leads to integrals that are quite involved. In contrast, FLAME schemes are very inexpensive and easy to construct.

Very closely related to the material of the present paper are the special difference schemes developed by Hadley [50,51] for electromagnetic wave propagation. In fact, these schemes are direct particular cases of FLAME, with Bessel functions forming a Trefftz-FLAME basis (although Hadley derives them from different considerations).

For unbounded domains, an artificial truncating boundary has to be introduced in FD and FE methods. The exact conditions at this boundary are nonlocal; however, local approximations are desirable to maintain the sparsity of the system matrix. One such approximation that has gained some popularity is the so-called "measured equation of invariance" (MEI) by Mei et al. [74,45,55]. As it happens, MEI can be viewed as a particular case of Trefftz-FLAME, with the basis functions taken as potentials due to some test distributions of sources (called '*metrons*' in MEI).

2.9. Special finite element methods

There is also quite a number of special finite elements, and related methods, that incorporate specific features of the solution. In problems of solid mechanics, Jirousek in the 1970s [62,61] proposed 'Trefftz' elements, with basis functions satisfying the underlying differential equation exactly. This not only improves the numerical accuracy substantially, but also reduces the Galerkin volume integrals in the computation of stiffness matrices to surface integrals (via integration by parts). Since then, Trefftz elements have been developed quite extensively; see a detailed study by Herrera [56] and a review paper by Jirousek and Zielinski [63].

Also in solid mechanics, Soh and Long [101] proposed two 2D elements with circular holes, while Meguid and Zhu [73] developed special elements for the treatment of inclusions.

Enrichment of FE bases with special functions is well established in computational mechanics. The variational multiscale method by Hughes [59] provides a general framework for adding fine-scale functions inside the elements to the usual coarse-scale FE basis. The additional amount of computational work is small if the fine scale bases are *local*, i.e. confined to the support of a single element. However, in this case the global effects of the fine scale are lost.

In the method of residual-free bubbles by Brezzi et al. [18], the standard element space is enriched with functions *satisfying the underlying differential equation* exactly. There is a similarity with the Trefftz schemes described in Section 4. However, the methods considered in the present paper are difference schemes rather than Galerkin finite element methods. The conformity of the method is maintained by having the 'bubbles' vanish at the interelement boundaries. Similar 'bubbles' are common in hierarchical finite element algorithms (see e.g. [123]); still, traditional FE methods – hierarchical or not – are built exclusively on piecewise-polynomial bases.

Farhat et al. [39] relax the conformity conditions and get higher flexibility of approximation in return. As in the case of residual-free bubbles, functions satisfying the differential equation are added to the FE basis. However, the continuity at interelement boundaries is only weakly enforced via Lagrange multipliers.

The following observation by Melenk [75] in reference to special finite elements is highly relevant to our discussion:

> "The theory of homogenization for problems with (periodic) microstructure, asymptotic expansions for boundary layers, and Kondrat'ev's corner expansions are a few examples of mathematical techniques yielding knowledge about the local properties of the solution. This knowledge may be used to construct local approximation spaces which can capture the behavior of the solution much more accurately than

the standard polynomials for a given number of degrees of freedom. Exploiting such information may therefore be much more efficient than the standard methods ...''

2.10. Domain decomposition

This section (added at the suggestion of the anonymous reviewer), unlike the previous ones, is intended to highlight the differences rather than the similarities between the methods of this paper and the existing techniques. The setup of FLAME (see the following section) may suggest its interpretation as a domain decomposition method. While this may be technically correct, there is a substantial conceptual and practical difference between the two classes of methods. In FLAME, the domain cover consists of 'micro' (stencil-size) subdomains. In contrast, domain decomposition methods usually operate with 'macro' subdomains that are relatively large compared to the mesh size. Consequently, the notions and ideas of domain decomposition (e.g. Schwartz methods, mortar methods, Chimera grids, and so on) will not be directly used in our development.

3. Variational-difference schemes with flexible local approximation

3.1. The model problem

The variational version of FLAME was described in [109,110]. This section follows [109] very closely; however, Section 3.2 is new. A new *non*variational version of FLAME is introduced in Section 4.

It was very recently brought to the author's attention [117] that the variational version of FLAME is very close to the ''meshless local Petrov–Galerkin'' (MLPG) method developed by Atluri and collaborators [4,3] (see also [69]). For the sake of completeness, this section briefly reviews the general setup of the method – in particular, the concept of multivalued approximation (that is not explicitly introduced in the literature on MLPG). This setup will be equally important for the nonvariational 'Trefftz' version of FLAME considered in Section 4.

Although the potential application areas of FLAME are broad, for illustrative purposes in this section we shall have in mind the model static Dirichlet problem

$$Lu \equiv -\nabla \cdot \sigma \nabla u = f \quad \text{in } \Omega \subset R^n \ \ (n = 2, 3); \quad u_{|\partial\Omega} = 0. \tag{5}$$

Here σ is a material parameter (conductivity, permittivity, permeability, etc.) that can be discontinuous across material boundaries and can depend on coordinates but not, in the linear case under consideration, on the potential u. The computational domain Ω is either two- or three-dimensional, with the usual mathematical assumption of a Lipschitz-continuous boundary. To simplify the exposition, precise mathematical definitions of the relevant functional spaces will not be given, and instead we shall assume that the solution has the degree of smoothness necessary to justify the analysis.

At any material interface boundary Γ, the usual conditions hold:

$$u_1 = u_2 \quad \text{on } \Gamma, \tag{6}$$

$$\sigma_1 \frac{\partial u_1}{\partial n} = \sigma_2 \frac{\partial u_2}{\partial n} \quad \text{on } \Gamma, \tag{7}$$

where the subscripts refer to the two subdomains Ω_1 and Ω_2 sharing the material boundary Γ, and n is the normal direction to Γ.

3.2. Motivating ideas

Intuitive ideas motivating the development of FLAME can be summarized as follows:

1. Flexible approximation vs. Taylor expansion.
2. Conformity of the method vs. flexibility of approximation.
3. Stencil as a "black box".

The first two items have already been discussed. The third one implies the treatment of the nodal values as combined inputs/outputs of a "black box". The relationship between these nodal values depends on the 'content' of the black box, i.e. on the distribution of material parameters near the stencil.

For example, if the standard 5-point stencil in 2D is located in a homogeneous region (i.e. $\sigma = \text{const.}$) with no sources ($f = 0$ in the vicinity of the stencil), the "black box" is approximately described by the discrete Laplace operator

$$\frac{u_{n_x-1,n_y} - 2u_{n_x,n_y} + u_{n_x+1,n_y}}{h_x^2} + \frac{u_{n_x,n_y-1} - 2u_{n_x,n_y} + u_{n_x,n_y+1}}{h_y^2} = 0, \tag{8}$$

where the notation for the nodal values of the solution is self-explanatory. Now suppose that the stencil is located near a material boundary (so that different nodes of the stencil may even lie in regions with different material characteristics). It is then intuitively clear that there "must be" a relationship similar to (8) between the nodal values – just with a different set of coefficients of the scheme. The only question is how to find this relationship. The answers given in this section and in [82] rely on variational principles. An alternative answer in the following section is based on 'Trefftz' approximations.

3.3. Construction of variational FLAME schemes

The first ingredient of the proposed setup is the same as in GFEM: a set of overlapping patches $\Omega^{(i)}$ covering the computational domain $\Omega = \cup\Omega^{(i)}$, $i = 1, 2, \ldots, n$. Within each patch, there is a local approximation space

$$\Psi^{(i)} = \text{span}\{\psi_\alpha^{(i)},\ \alpha = 1, 2, \ldots, m^{(i)}\}. \tag{9}$$

Note that no *global* approximation space will be considered. Rather, the following notion is introduced:

For a given domain cover $\{\cup\Omega^{(i)}\}$ with corresponding local spaces $\Psi^{(i)}$, a *multivalued approximation* $u_h\{\cup\Omega^{(i)}\}$ of a given potential u is just a collection of patch-wise approximations:

$$u_h\{\bigcup \Omega^{(i)}\} \equiv \{u_h^{(i)} \in \Psi^{(i)}\}. \tag{10}$$

In regions where two or more patches overlap (Fig. 3), several local approximations coexist and do not have to be the same. This situation in fact is inherent in the FD methodology but is almost never stated explicitly.[3]

The second ingredient is a set of n nodes (the number of nodes is equal to the number of patches). Although a meshless setup is possible, we shall for maximum simplicity assume a regular grid with a mesh size h. The ith stencil is defined as a set of $m^{(i)}$ nodes within $\Omega^{(i)}$: $\text{Stencil}^{(i)} \equiv \{\text{nodes} \in\ \Omega^{(i)}\}$. For

[3] One might argue that in FD methods approximation between the nodes is not multivalued but simply undefined. This point of view is not incorrect but ignores the fact that the very derivation of FD schemes typically relies upon disparate Taylor expansions in the neighborhoods of each grid point.

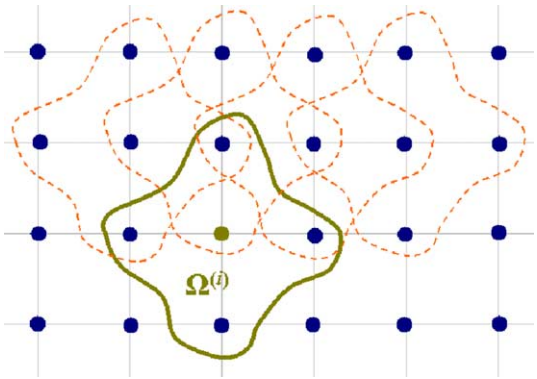

Fig. 3. Overlapping patches with 5-point stencils. (Reprinted by permission from [109] ©2004 IEEE.)

any continuous potential u, $\mathcal{N}u$ will denote the set of its values at all grid nodes (viewed as a Euclidean vector in R^n), and $\mathcal{N}^{(i)}u$ – the set of nodal values on Stencil$^{(i)}$. Convergence in this framework (for $h \to 0$) is understood either in the nodal norm as $\|u_h - \mathcal{N}u\|_{E^n} \to 0$ or, alternatively, in the Sobolev norm as $(\sum_i \|u_h^{(i)} - u\|^2_{H^1(\Omega^{(i)})})^{1/2} \to 0$. The underscore signs throughout the paper denote column vectors.

The next ingredient in the variational formulation is a set of linear test functionals that will be denoted with primes:

$$\{(\psi^{(i)})'\}, \quad \omega^{(i)} \equiv \mathrm{supp}(\psi^{(i)'}) \subset\subset \Omega^{(i)}, \quad i = 1, 2, \ldots n. \tag{11}$$

Since $\psi^{(i)'}$ vanishes outside $\Omega^{(i)}$, possible discontinuity of the local approximation $u_h^{(i)}$ at the patch boundary is unimportant. The local solution within the ith patch is a linear combination of the chosen basis functions:

$$u_h^{(i)} = \sum_{\alpha=1}^{m^{(i)}} c_\alpha^{(i)} \psi_\alpha^{(i)} = \underline{c}^{(i)T} \underline{\psi}^{(i)} \in \Psi^{(i)}, \tag{12}$$

where $\underline{c}^{(i)}$, $\underline{\psi}^{(i)}$ are viewed as column vectors, with their individual entries marked with subscript α. In the variational formulation, the discrete system of equations is obtained by applying the chosen linear test functionals to the differential equation:

$$[u_h^{(i)}, (\psi^{(i)})'] = \langle f, (\psi^{(i)})' \rangle \tag{13}$$

or equivalently

$$[\underline{c}^{(i)\mathrm{T}} \underline{\psi}^{(i)}, (\psi^{(i)})'] = \langle f, (\psi^{(i)})' \rangle, \tag{14}$$

where $[u, w] \equiv (Lu, w)$ and $\langle f, (\psi^{(i)})' \rangle$ is an alternative notation for $(\psi^{(i)})'(f)$.

This equation is in terms of the expansion coefficients c of (12). To obtain the actual difference scheme in terms of *the nodal values*, one needs to relate the coefficient vector $\underline{c}^{(i)} \equiv \{c_\alpha^{(i)}\} \in R^m$ of expansion (12) to the vector $\underline{u}^{(i)} \in r^M$ of the nodal values of $u_h^{(i)}$ on Stencil$^{(i)}$. (The superscript (i) for M and m has been dropped for simplicity of notation.) The relevant transformation matrix

$$\underline{u}^{(i)} = N^{(i)} \underline{c}^{(i)} \tag{15}$$

contains the nodal values of the basis functions on the stencil; if r_k is the position vector of node k, then

$$N^{(i)} = \begin{pmatrix} \psi_1^{(i)}(r_1) & \psi_2^{(i)}(r_1) & \dots & \psi_m^{(i)}(r_1) \\ \psi_1^{(i)}(r_2) & \psi_2^{(i)}(r_2) & \dots & \psi_m^{(i)}(r_2) \\ \dots & \dots & \dots & \dots \\ \psi_1^{(i)}(r_M) & \psi_2^{(i)}(r_M) & \dots & \psi_m^{(i)}(r_M) \end{pmatrix}. \tag{16}$$

If $M = m$ and $N^{(i)}$ is nonsingular,

$$\underline{c}^{(i)} = (N^{(i)})^{-1}\underline{u}^{(i)} \tag{17}$$

and (14) becomes

$$[\underline{u}^{(i)\mathrm{T}}(N^{(i)})^{-\mathrm{T}}\underline{\psi}^{(i)}, (\psi^{(i)})'] = \langle f, (\psi^{(i)})'\rangle. \tag{18}$$

(It is implied that the functional [,] in the left-hand side is applied to the column vector $\{\underline{\psi}^{(i)}\}$ entry-wise). Then (14) or (18) can equally well be written as

$$\underline{u}^{(i)\mathrm{T}}(N^{(i)})^{-\mathrm{T}}[\underline{\psi}^{(i)}, (\psi^{(i)})'] = \langle f, (\psi^{(i)})'\rangle. \tag{19}$$

Equivalently, one may note that matrix N governs the transformation from the original basis $\{\psi_\alpha^{(i)}\}$ in $\Psi^{(i)}$ to the nodal basis $\{\underline{\psi}_{\mathrm{nodal}}^{(i)}\}$ such that $\psi_{\alpha\beta,\mathrm{nodal}}^{(i)}(r_\beta) = \delta_{\alpha\beta}$. Indeed, two equivalent representations of $u_h^{(i)}$ in the original and nodal bases

$$u_h^{(i)} = \underline{u}^{(i)\mathrm{T}}\underline{\psi}_{\mathrm{nodal}}^{(i)} = \underline{c}^{(i)\mathrm{T}}\underline{\psi}^{(i)} \tag{20}$$

yield, together with (17),

$$\underline{\psi}_{\mathrm{nodal}}^{(i)} = (N^{(i)})^{-T}\underline{\psi}^{(i)} \tag{21}$$

which reveals that (14) is in fact

$$\underline{u}^{(i)\mathrm{T}}[\underline{\psi}_{\mathrm{nodal}}^{(i)}, (\psi^{(i)})'] = \langle f, (\psi^{(i)})'\rangle. \tag{22}$$

Expressions (18) and (22) are equivalent but suggest two different algorithmic implementations of the difference scheme. According to (18), one can first compute the Euclidean vector of inner products $\underline{\zeta}^{(i)} = [\underline{\psi}^{(i)}, (\psi^{(i)})']$ and the difference scheme then is $(N^{(i)})^{-\mathrm{T}}\underline{\zeta}^{(i)}$. Alternatively, according to (22), one first computes the nodal basis (21) and then the products $[\underline{\psi}_{\mathrm{nodal}}^{(i)}, (\psi^{(i)})']$.

The algorithm for generating variational-difference schemes for an equation $Lu = f$ can be summarized as follows (for $M = m$ and nonsingular $N^{(i)}$):

1. For a given node, choose a stencil, a set of local approximating functions $\{\psi\}$, and a test functional ψ'.
2. Calculate the values of the ψ's at the nodes and combine these values into the N matrix (16).
3. Solve the system with matrix N^{T} and the r.h.s. ψ to get the nodal basis.
4. Compute the coefficients of the difference scheme as $[\psi_{\mathrm{nodal}}, \psi'] \equiv (L\psi_{\mathrm{nodal}}, \psi')$.

Alternatively, stages 3 and 4 can be switched:

3′. Compute the values $[\psi, \psi'] \equiv (L\psi, \psi')$.
4′. Solve the system with matrix N^{T} and the r.h.s. $[\psi, \psi']$ to obtain the coefficients of the difference scheme.

Note that the r.h.s. of the system of equations involves *functions* $\{\underline{\psi}_{\mathrm{nodal}}\}$ in the first version of the algorithm and *numbers* $[\underline{\psi}, \psi']$ in the second version. While working with numbers is easier, the nodal functions can be useful and may be reused for different test functionals.

Variational-difference schemes (18) and (22) are consistent essentially by construction [109] (see also Sections 4.4 and 4.5 for related proofs).

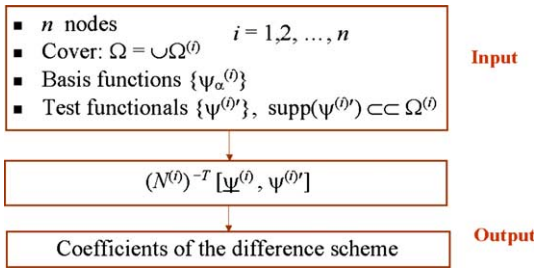

Fig. 4. A 'machine' for variational-difference FLAME schemes. (Reprinted by permission from [109] ©2004 IEEE.)

Graphically, the procedure can be viewed as a "machine" for generating variational-difference FLAME schemes (Fig. 4).

Remark 1. With this generic setup, no blanket claim of convergence of the variational scheme can be made. The difference scheme is consistent by construction [109] but its stability needs to be examined in each particular case.

Remark 2. Implementation of (18) or (22) implies solving a small system of linear equations whose dimension is equal to the stencil size.

Volume integration in (18) is avoided if the test functional is taken to be either the Dirac delta or, alternatively, the characteristic ("window") function $\Pi(\omega^{(i)})$ of some domain $\omega^{(i)} \subset\subset \Omega^{(i)}$: that is, $\Pi(\omega^{(i)} = 1$ inside $\omega^{(i)}$ and zero outside. With the "window" function, one arrives at a control volume (flux balance) scheme with surface integration. (Typically, $\omega^{(i)}$ is the same size as a grid cell but centered at a node.) The computational cost is asymptotically proportional to the number of grid nodes but depends on the numerical quadratures used to compute the surface fluxes.

3.4. Summary of the variational-difference setup

The setup of variational FLAME schemes can be summarized as follows:

- A system of overlapping patches is introduced.
- Desired approximating functions are used within each patch, independently of other patches.
- Simple regular grids can be used.
- When patches overlap, the approximation is generally multivalued (as is also the case in standard FD analysis).
- The nodal solution on the grid is single-valued and provides the necessary "information transfer" between the overlapping patches.
- Since a unique globally continuous interpolant is not defined, the Galerkin method in $H^1(\Omega)$ is generally not applicable. However, within each patch there is a sufficiently smooth local approximation (12), and a general moment (weighted residual) method can be applied, provided that the support of the test function is contained entirely within the patch.

In particular, by introducing the standard 'control volume' box centered at a given node of the grid and setting the test function equal to one within that control volume and zero elsewhere, one arrives at a flux balance scheme. This is a generalization of the standard 'control volume' technique to any set of suitably defined local approximating functions. Only surface integrals, rather than volume quadratures, are needed, which greatly reduces the computational overhead.

Application examples of the variational-difference version of FLAME were already given in [109]. We now turn to the nonvariational version that in many respects is more appealing.

4. Non-variational Trefftz-FLAME schemes with flexible local approximation

4.1. Construction of the nonvariational schemes

The schemes described in this section are much simpler and yet in many cases more efficient and accurate than the variational-difference schemes considered previously. The overall setup is conceptually the same as before: the computational domain Ω is covered with a set of overlapping 'patches' (subdomains) $\Omega^{(i)}$; each patch contains a stencil of an auxiliary global Cartesian (for simplicity) grid.

Let us initially assume that the underlying differential equation within a patch $\Omega^{(i)}$ is homogeneous:

$$Lu = 0 \quad \text{in } \Omega^{(i)}, \tag{23}$$

where L is a differential operator (one may want to have in mind the elliptic Eq. (5) as an example).

Within each patch, the approximate solution $u_h^{(i)}$ is sought as a linear combination of $m^{(i)}$ basis functions $\{\psi_\alpha^{(i)}\}$ (12) (repeated here for easy reference):

$$u_h^{(i)} = \sum_\alpha c_\alpha^{(i)} \psi_\alpha^{(i)}. \tag{24}$$

The novelty now is that we consider *Trefftz* methods, where the approximating functions $\psi^{(i)}$ *satisfy the underlying differential equation* (23) *exactly*. Trefftz methods are well known in the variational context [56]; in contrast, here a purely *finite-difference* approach is taken and will prove to be attractive in a variety of cases.[4]

As before (see Section 3.3), the relationship between the vectors of coefficients $\underline{c}^{(i)}$ and the nodal values is

$$N^{(i)} \underline{c}^{(i)} = \underline{u}^{(i)}, \tag{25}$$

where matrix $N^{(i)}$ (16) comprises the nodal values of all basis functions at all stencil points.

In the Trefftz version, since the basis functions by construction already satisfy the underlying differential equation, so does the approximate solution $u_h^{(i)}$, automatically. Therefore there is no need to apply a functional as in (13), (14), (18) and (22) to test this solution, which is a major simplification. In the nonvariational Trefftz-FLAME schemes there will typically be fewer approximating functions than nodes within the patch – most frequently, m functions for $M = m + 1$ stencil nodes. The nodal matrix $N^{(i)}$ is thus in general rectangular. (Compare this with the *variational*-difference formulation of the previous section, where the number of basis functions is typically equal to the number of nodes.) The number of approximating functions may be different for different patches, but for brevity of notation this is not explicitly indicated.

In the simplest illustrative 1D example, with $m = 2$ basis functions $\psi_{1,2}$ at three grid points x_{i-1}, x_i, x_{i+1}, matrix $N^{(i)}$ is

$$N^{(i)} = \begin{pmatrix} \psi_1(x_{i-1}) & \psi_2(x_{i-1}) \\ \psi_1(x_i) & \psi_2(x_i) \\ \psi_1(x_{i+1}) & \psi_2(x_{i+1}) \end{pmatrix}. \tag{26}$$

[4] The starting point for the author's development of Trefftz-FLAME schemes was Gary Friedman's nonvariational version of FLAME for unbounded problems [42,52].

Since there are only two independent parameters (coefficients in the linear combination of $\psi_{1,2}$), the three nodal values on the stencil must be linearly related: $s_{-1}u_{i-1} + s_0 u_i + s_{+1}\, u_{i+1} = 0$ for some coefficients s_0, $s_{\pm 1}$. More generally for an M-point stencil, a vector of coefficients $\underline{s}^{(i)} \in R^M$ of the difference scheme is sought to yield

$$\underline{s}^{(i)\mathrm{T}}\underline{u}^{(i)} = 0 \tag{27}$$

for the nodal values $\underline{u}^{(i)}$ of *any* function $u_h^{(i)}$ of form (24). Throughout the paper, vector $\underline{s}^{(i)}$ is treated as a column matrix. Due to (25) and (27),

$$\underline{s}^{(i)\mathrm{T}}N^{(i)}\underline{c}^{(i)} = 0. \tag{28}$$

For this to hold for any set of coefficients $\underline{c}^{(i)}$, one must have

$$\underline{s}^{(i)} \in \mathrm{Null}(N^{(i)\mathrm{T}}). \tag{29}$$

If the null space is of dimension one, $\underline{s}^{(i)}$ represents the desired scheme (up to an arbitrary factor), and (29) is the principal expression of the Trefftz-FLAME scheme. The meaning of (29) is quite simple: each equation in the system $N^{(i)\mathrm{T}}\underline{s}^{(i)} = 0$ implies that the respective basis function satisfies the difference scheme with coefficients $\underline{s}^{(i)}$. There is thus an elegant duality feature between the continuous and discrete problems: any linear combination of the basis functions satisfies both the differential equation (due to the choice of the 'Trefftz' basis) *and* the difference equation with coefficients $\underline{s}^{(i)}$.

As we shall see in Section 4, definition (29), despite its simplicity, is surprisingly rich. For different choices of basis functions and stencils it gives rise to a variety of difference schemes.

While there is no obvious way to determine the dimension of the null space in (29) a priori, for several classes of problems considered later the dimension is indeed one. If the null space is empty, the construction of the Trefftz-FLAME scheme fails, and one may want to either increase the size of the stencil or reduce the basis set. If the dimension of the null space is greater than one, there are two general options. First, the stencil and/or the basis can be adjusted. Second, one may use the additional freedom in the choice of the coefficients $\underline{s}^{(i)}$ to seek an "optimal" (in some sense) scheme as a linear combination of the independent null space vectors. For example, it may be desirable to find a diagonally dominant scheme.

An alternative interpretation of (29) is that $\underline{s}^{(i)}$ is orthogonal to the image of $N^{(i)}$ due to (28), hence $\underline{s}^{(i)}$ is in the null space of $N^{(i)\mathrm{T}}$. In the complex case, though, orthogonality should not be understood in terms of the standard complex inner product which, unlike (28), includes conjugates.

Once the basis and the stencil are chosen, the Trefftz-FLAME scheme is generated in a very simple way:

- Form matrix $N^{(i)}$ of the nodal values of the basis functions.
- Find the null space of $N^{(i)\mathrm{T}}$.

Proposition 1. *The Trefftz-FLAME scheme defined by (29) is invariant with respect to the choice of the basis in the local space* $\Psi^{(i)} \equiv \mathrm{span}\{\psi_\alpha^{(i)}\}$.

Proof. A linear transformation of the ψ-basis replaces N^{T} with QN^{T}, where Q is a nonsingular matrix, which does not affect the null space. □

The algorithm is much simpler and yet in many cases more effective (see examples below) than the variational version of FLAME. It can be sketched as a 'machine' for generating Trefftz-FLAME schemes (Fig. 5). As in the variational version, it should be stressed that the algorithm is heuristic and no blanket claim of convergence can be made. The schemes need to be considered on a case-by-case basis, which is done for a variety of problems in Section 4. However, consistency can be proven (Section 4.4) in general, and convergence then follows for the subclass of schemes with a monotone difference operator (Section 4.5). Construction of monotone Trefftz-FLAME schemes for electromagnetic multiparticle problems is discussed in [111].

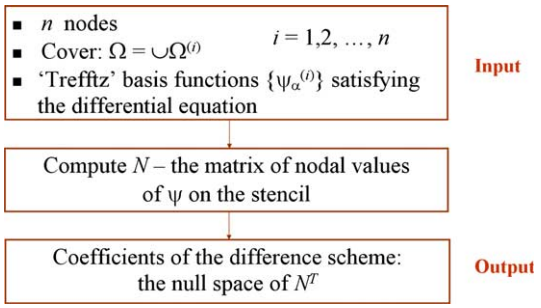

Fig. 5. A 'machine' for Trefftz-FLAME schemes: the algorithm is substantially simpler than the variational version. (Reprinted by permission from [111] ©2005 IEEE.)

4.2. The treatment of boundary conditions

Note that in the FLAME framework approximations over different stencils are completely independent from one another. Therefore, if the domain boundary conditions are of standard types and no special behavior of the solution at the boundaries is manifest, one can simply employ any standard FD scheme at the boundary.[5]

If the solution is known to exhibit some special features at the boundary, it may be possible to incorporate these features into the FLAME scheme. One example is perfectly matched layers (PML) for electromagnetic and acoustic wave propagation considered briefly in Section 5.10 and in some more detail in [111]. The research on FLAME-PML conditions is ongoing.

4.3. Trefftz-FLAME schemes for inhomogeneous and nonlinear equations

So far we considered Trefftz-FLAME schemes only for homogeneous equations (i.e. with the zero right-hand side within a given patch). For inhomogeneous equations of the form

$$Lu = f \quad \text{in } \Omega^{(i)} \tag{30}$$

a natural approach is to split the solution up into a particular solution $u_f^{(i)}$ of the inhomogeneous equation and the remainder $u_0^{(i)}$ satisfying the homogeneous one:

$$u = u_0^{(i)} + u_f^{(i)}, \tag{31}$$

$$Lu_0^{(i)} = 0; \quad Lu_f^{(i)} = f. \tag{32}$$

Superscript (i) emphasizes that the splitting is *local*, i.e. needs to be introduced only within its respective patch $\Omega^{(i)}$ containing the grid stencil around node i. Since $u_f^{(i)}$ is local (and in particular need not satisfy any exterior boundary conditions), it is usually relatively easy to construct.

Let a Trefftz-FLAME scheme $\underline{s}^{(i)}$ be generated for a given set of basis functions and assume that the consistency error ϵ for this scheme tends to zero as $h \to 0$; that is,

$$\underline{s}^{(i)\mathrm{T}} \mathcal{N}^{(i)} u_0^{(i)} = \epsilon \equiv \epsilon\left(h, u_0^{(i)}\right) \to 0 \quad \text{as grid size } h \to 0, \tag{33}$$

where $\mathcal{N}^{(i)}$, as before, denotes the nodal values of a function on stencil (i). Then clearly

[5] Since most Taylor-based schemes are particular cases of FLAME (with polynomial basis functions), it would be technically correct to say that the whole set of difference equations, including the treatment of boundary conditions, is based on FLAME schemes.

$$\underline{s}^{(i)\mathrm{T}}\mathcal{N}^{(i)}u = \underline{s}^{(i)\mathrm{T}}\mathcal{N}^{(i)}u_0 + \underline{s}^{(i)\mathrm{T}}\mathcal{N}^{(i)}u_f = \underline{s}^{(i)\mathrm{T}}\mathcal{N}^{(i)}u_f + \epsilon.$$

This immediately implies that the consistency error of the difference scheme

$$\underline{s}^{(i)\mathrm{T}}\underline{u}_h = \underline{s}^{(i)\mathrm{T}}\mathcal{N}^{(i)}u_f \tag{34}$$

is ϵ, i.e. exactly the same as for the homogeneous case. (The Euclidean vector $\underline{u}_h$ of nodal values does not need the superscript because the nodal values are unique and do not depend on the patch.) Note that there are absolutely no constraints on the smoothness of $u_f^{(i)}$, provided that its nodal values are well defined. The particular solution $u_f^{(i)}$ can even be singular as long as the singularity point does not coincide with a grid node. For example, in [108] difference schemes of this kind were constructed for the Coulomb potential of point charges. An electrostatic problem with a line charge source is solved in a similar way in [111].

For *nonlinear* problems, the Newton–Raphson method is traditionally used for the *discrete* system of equations. In connection with FLAME schemes, Newton–Raphson–Kantorovich iterations are applied to the original continuous problem rather than the discrete one. Let the equation be

$$Lu = f, \tag{35}$$

where L is a differentiable operator. The $(k+1)$th approximation u_{k+1} to the exact solution is obtained from the kth approximation u_k by linearization in the following way. If $u = u_k + \delta u$,

$$Lu = L(u_k + \delta u) = Lu_k + L'(u_k)\delta u + \mathrm{o}(\|\delta u\|), \tag{36}$$

where L' is the Fréchet derivative of L. Ignoring higher-order terms, one gets an approximation δu_k for δu by solving the linear system

$$L'(u_k)\delta u_k = f - Lu_k \tag{37}$$

and then updates the solution:

$$u_{k+1} = u_k + \delta u_k. \tag{38}$$

Equivalently,

$$u_{k+1} = u_k + (L'(u_k))^{-1}(f - Lu_k). \tag{39}$$

Along with an initial guess u_0, iterative process (37), (38) – or just (39) – defines the Newton–Raphson–Kantorovich algorithm. Trefftz-FLAME schemes can then be applied to L' (which of course is a linear operator by definition), provided that a suitable set of local approximating functions can be found.

4.4. Consistency of the schemes

Let us rewrite the patch-wise difference equation (34) in matrix form as a global system of difference equations for the underlying differential equation $Lu = f$:

$$L_h\underline{u}_h = \underline{f}_h \quad \text{with } \underline{f}_{hi} = \underline{s}^{(i)\mathrm{T}}\mathcal{N}^{(i)}u_f^{(i)} \tag{40}$$

(if the differential equation is homogeneous within the patch, then $u_f^{(i)} = 0$). Note that the ith row of matrix L_h contains the coefficients of scheme $\underline{s}^{(i)\mathrm{T}}$ and, in addition, a (large) number of zero entries. We shall assume that the equations can be scaled in such a way that

$$c_1 f(r) \leqslant \underline{f}_{hi} \leqslant c_2 f(r) \quad \forall r \in \Omega^{(i)}, \;\; c_{1,2} > 0, \tag{41}$$

where $c_{1,2}$ do not depend on i and h. This scaling is important because otherwise e.g. the meaningless scheme $h^{100}u_i = 0$ would technically be consistent (as defined below) for *any* differential equation.

The consistency error of scheme (34) and (40) is, by definition, obtained by substituting the nodal values of the exact solution u^* into the difference equation. We shall call this scheme consistent if, with scaling (41), the following condition holds:

$$\text{consistency error} \equiv \epsilon_c(h) = \max_i \left| \underline{s}^{(i)\mathrm{T}} \mathcal{N}^{(i)} u^* - \underline{f}_{hi} \right| = \max_i \left| \underline{s}^{(i)\mathrm{T}} (\mathcal{N}^{(i)} u^* - \underline{u}_{hi}) \right| \to 0 \quad \text{as } h \to 0. \tag{42}$$

For FLAME schemes, consistency follows directly from the approximation properties of the basis set as long as (41) holds. Indeed, let $\epsilon_a(h)$ be the approximation error of the "homogeneous part" $u_0^{(i)}$ of the exact solution u^* in a patch $\Omega^{(i)}$:

$$\epsilon_a(h) = \min_{c^{(i)} \in R^m} \left\| u^* - u_f^{(i)} - \sum_{\alpha=1}^{m} c_\alpha^{(i)} \psi_\alpha^{(i)} \right\|_\infty . \tag{43}$$

Equivalently, there exists a coefficient vector $\underline{c}^{(i)} \in R^m$ such that

$$u^* = u_f^{(i)} + \sum_{\alpha=1}^{m} c_\alpha^{(i)} \psi_\alpha^{(i)} + \eta, \quad \|\eta\|_\infty = \epsilon_a(h). \tag{44}$$

For the nodal values, one then has due to (25)

$$\mathcal{N}^{(i)} u^* = \mathcal{N}^{(i)} u_f^{(i)} + N^{(i)} \underline{c}^{(i)} + \underline{\eta} \tag{45}$$

where $\underline{\eta} = \mathcal{N}^{(i)} \eta$ is the vector of nodal values of η on stencil i and $N^{(i)}$ is (as always) the matrix of nodal values of the basis functions. Due to (44),

$$\|\underline{\eta}\|_\infty \leqslant \epsilon_a(h)$$

and due to (45), the consistency error for scheme (40) with coefficients (29) is

$$\begin{aligned} |\epsilon_c(h)| &= \max_i \left| \underline{s}^{(i)\mathrm{T}} \mathcal{N}^{(i)} u^* - \underline{s}^{(i)\mathrm{T}} \mathcal{N}^{(i)} u_f^{(i)} \right| = \max_i \left| \underline{s}^{(i)\mathrm{T}} (N^{(i)} \underline{c}^{(i)} + \underline{\eta}) \right| = \max_i \left| \underline{s}^{(i)\mathrm{T}} N^{(i)} \underline{c}^{(i)} + \underline{s}^{(i)\mathrm{T}} \underline{\eta} \right| \\ &= \max_i \left| \underline{s}^{(i)\mathrm{T}} \underline{\eta} \right| \leqslant M \epsilon_a(h), \end{aligned} \tag{46}$$

which shows that the consistency error is bounded by the approximation error.

4.5. Convergence of the schemes

For conventional difference schemes and the Poisson equation, convergence is proved in standard texts (e.g. [80] or [104]). Following the substance of these proofs, one arrives at a more general convergence result (Theorem 1 below). The following lemma will be needed.

Lemma 1. *If the scheme is scaled according to (41) and the consistency condition (42) holds, there exists a reference nodal vector $\underline{u}_{1h}$ such that*

$$\underline{u}_{1h} \leqslant U_1 \quad \textit{and} \quad L_h \underline{u}_{1h} \geqslant \sigma_1 > 0 \tag{47}$$

with numbers U_1 and σ_1 independent of h. (All vector inequalities are understood entry-wise.)

[A remark on notation: subscript 1 is meant to show that, as seen from the proof below, the auxiliary potential u_{1h} may be related to the solution of the differential equation with the unit right-hand side.]

Proof. The reference potential u_{1h} can be found explicitly by considering the auxiliary problem

$$L u_1 = 1 \tag{48}$$

with the same boundary conditions as the original problem. Condition (42) applied to the nodal values of u_1 implies that for sufficiently small h the consistency error will fall below $\frac{1}{2}c_1$, where c_1 is the parameter in (41):

$$\left|\underline{s}^{(i)\mathrm{T}}\mathscr{N}^{(i)}u_1 - f_{hi}\right| \leqslant \frac{1}{2}c_1.$$

Therefore, since $f = 1$ in (41),

$$|\underline{s}^{(i)\mathrm{T}}\mathscr{N}^{(i)}u_1| \geqslant |f_{hi}| - \left|f_{hi} - \underline{s}^{(i)\mathrm{T}}\mathscr{N}^{(i)}u_1\right| \geqslant c_1 - \frac{1}{2}c_1 = \frac{1}{2}c_1 \tag{49}$$

(the vector inequality is understood entry-wise). Thus one can set $\underline{u}_{1h} = L_h\mathscr{N}u_1$, with $\sigma_1 = \frac{1}{2}c_1$ and $U_1 = \|u_1\|_\infty$. □

Theorem 1. *Let the following conditions hold for difference schemes* (34) and (40):

1. *Consistency in the sense of* (42) and (41).
2. *Monotonicity*: *if* $L_h\underline{x} \geqslant 0$, *then* $\underline{x} \geqslant 0$. (50)

Then the numerical solution converges in the nodal norm, and

$$\|\underline{u}_h - \mathscr{N}u^*\|_\infty \leqslant \epsilon_c U_1/\sigma_1, \tag{51}$$

where σ_1 *is the parameter in* (47).

Proof. Let $\underline{\epsilon}_h = \underline{u}_h - \mathscr{N}u^*$. By consistency,

$$L_h\underline{\epsilon}_h \leqslant \epsilon_c \leqslant \epsilon_c L_h\underline{u}_{1h}/\sigma_1 = L_h(\epsilon_c\underline{u}_{1h}/\sigma_1),$$

where (47) was used. Hence due to monotonicity

$$\epsilon_h \leqslant \epsilon_c\underline{u}_{1h}/\sigma_1. \tag{52}$$

It then also follows that

$$\epsilon_h \geqslant -\epsilon_c\underline{u}_{1h}/\sigma_1. \tag{53}$$

Indeed, if that were not true, one would have $(-\epsilon_h) \geqslant \epsilon_c\underline{u}_{1h}/\sigma_1$, which would contradict the error estimate (52) for the system with $(-\underline{f})$ instead of $\underline{f}$ in the right-hand side. □

Diagonal dominance of matrix L_h is known to be a sufficient condition for monotonicity if the diagonal entries of L_h are positive and the off-diagonal ones are nonpositive [113,114]. As a measure of the relative magnitude of the diagonal elements, one can use

$$\min_i \frac{|L_{h,ii}|}{\sum_j |L_{h,ij}|} \tag{54}$$

with matrix L_h being diagonally dominant for $q = 0.5$ and diagonal for $q = 1$.

Diagonal dominance is a strong condition that does not hold in general. However, diagonally dominant Trefftz-FLAME schemes can be constructed for electro- and magnetostatic multiparticle problems of Section 5.10 [111].

Not surprisingly, estimate (51) is the ratio of approximation and stability parameters. Even if the monotonicity condition of the theorem is not satisfied, this estimate may still be useful as a heuristic criterion, with the value of q (54) monitored in the actual computation. The approximation accuracy ϵ_a is key. In fact,

the 'Trefftz' bases are effective not just because they (by definition) satisfy the underlying differential equation, but because they happen to have superior approximation properties in many cases (see e.g. Section 5.5 and 5.6).

5. Trefftz-FLAME schemes: case studies

5.1. The 1D Laplace equation

Obviously, the 1D Laplace equation is trivial and is used here only to provide the simplest possible example of Trefftz-FLAME schemes. For convenience, consider a uniform grid with size h, choose a 3-point stencil and place the origin at the middle node. Two basis functions satisfying the Laplace equation are

$$\psi_1 = 1; \quad \psi_2 = x.$$

Then, since the coordinates of the stencil nodes are $[-h, 0, h]$, the (transposed) nodal matrix (16) is

$$N^{\mathrm{T}} = \begin{pmatrix} 1 & 1 & 1 \\ -h & 0 & h \end{pmatrix}$$

and the Trefftz-FLAME difference scheme is[6]

$$\underline{s} = \mathrm{Null}(N^{\mathrm{T}}) = [1, -2, 1] \quad \text{(times an arbitrary coefficient)},$$

which coincides with the standard 3-point scheme for the Laplace equation.

5.2. The 1D Helmholtz and convection–diffusion equations

A less trivial case is the 1D Helmholtz equation

$$\frac{\mathrm{d}^2 u}{\mathrm{d}x^2} - \kappa^2 u = 0$$

with any complex κ. Let us choose the same 3-point stencil $[-h, 0, h]$ as before and two basis functions satisfying the Helmholtz equation:

$$\psi_1 = \exp(\kappa x); \quad \psi_2 = \exp(-\kappa x).$$

Then the matrix of nodal values (16) is

$$N^{\mathrm{T}} = \begin{pmatrix} \exp(-\kappa h) & 1 & \exp(\kappa h) \\ \exp(\kappa h) & 1 & \exp(-\kappa h) \end{pmatrix}$$

and the resultant difference scheme is

$$\underline{s} = \mathrm{Null}(N^{\mathrm{T}}) = [1, -2\cosh(\kappa h), 1]. \tag{55}$$

Since the theoretical solution in this 1D case is exactly representable as a linear combination of the chosen basis functions, the difference scheme yields the exact solution (in practice, up to the round-off error). This scheme is known and has been derived in a different way by Mickens [78] (see also [39,53]).

[6] As a slight abuse of notation, the square-bracketed arrays (such as $[1, -2, 1]$) do not distinguish between row and column vectors.

Quite similarly, for the 1D convection–diffusion equation with constant coefficients

$$D\frac{\mathrm{d}^2u}{\mathrm{d}x^2} - b\frac{\mathrm{d}u}{\mathrm{d}x} = 0, \quad D > 0$$

one has two 'Trefftz' basis functions:

$$\psi_1 = 1; \quad \psi_2 = \exp(qx), \quad q = b/D.$$

For the 3-point stencil $[-h, 0, h]$, the (transposed) matrix of nodal values (16) is

$$N^{\mathrm{T}} = \begin{pmatrix} 1 & 1 & 1 \\ \exp(-qh) & 1 & \exp(qh) \end{pmatrix}$$

and the Trefftz-FLAME difference scheme is

$$\underline{s} = \mathrm{Null}(N^{\mathrm{T}}) = \left[\frac{\exp(qh)}{\exp(qh)-1}, -\frac{\exp(qh)+1}{\exp(qh)-1}, \frac{1}{\exp(qh)-1}\right] \tag{56}$$

(up to an arbitrary factor). This coincides (in the case of the homogeneous convection–diffusion equation with constant coefficients) with the well-known exponentially fitted scheme (see e.g. [102,92,88]).

5.3. The 1D heat equation with variable material parameter

Consider the 1D homogeneous heat conduction equation:

$$\frac{\mathrm{d}}{\mathrm{d}x}\left(\lambda(x)\frac{\mathrm{d}u}{\mathrm{d}x}\right) = 0, \tag{57}$$

where $\lambda(x)$ is the material parameter. Two approximating functions for the FLAME-Trefftz scheme can be chosen as linearly independent solutions of this equation on the interval $[x_{k-1}, x_{k+1}]$:

$$\psi_1 = 1, \quad \psi_2 = \int_{x_k}^{x} \lambda^{-1}(\xi)\,\mathrm{d}\xi.$$

With this basis, the transposed nodal matrix (16) for the stencil $[x_{k-1}, x_k, x_{k+1}]$ is

$$N^{\mathrm{T}} = \begin{pmatrix} 1 & 1 & 1 \\ -\Sigma_{k-1} & 0 & \Sigma_{k+1} \end{pmatrix},$$

where $\Sigma_{k-1} = \int_{x_{k-1}}^{x_k} \lambda^{-1}(\xi)\,\mathrm{d}\xi$, $\Sigma_{k+1} = \int_{x_k}^{x_{k+1}} \lambda^{-1}(\xi)\mathrm{d}\xi$ have the physical meaning of thermal resistances of the respective segments. The difference scheme is, up to an arbitrary factor,

$$\underline{s} = \mathrm{Null}(N^{\mathrm{T}}) = [-\Sigma_{k-1}^{-1}, \Sigma_{k-1}^{-1} + \Sigma_{k+1}^{-1}, -\Sigma_{k+1}^{-1}], \tag{58}$$

which has a clear interpretation as a flux balance equation:

$$\Sigma_{k-1}^{-1}(u_k - u_{k-1}) + \Sigma_{k+1}^{-1}(u_k - u_{k+1}) = 0.$$

Such schemes are indeed typically derived from flux balance considerations (see e.g. the "homogeneous schemes" in [95]) but, as we can now see, are a natural particular case of Trefftz-FLAME.

If the integrals in the expressions for thermal resistances Σ can be calculated exactly, the scheme is itself exact, i.e. the consistency error is zero (the theoretical solution satisfies the FD equation). This holds even if the material parameter λ is discontinuous.

5.4. The 2D and 3D laplace equation

Consider a regular rectangular grid, for simplicity with spacing h the same in both directions, and the standard 5-point stencil. The origin of the coordinate system is placed for convenience at the central node

of the stencil. With four basis functions $[1, x, y, x^2 - y^2]$ satisfying the Laplace equation, the nodal matrix (16) becomes

$$N^{\mathrm{T}} = \begin{pmatrix} 1 & 1 & 1 & 1 & 1 \\ 0 & -h & 0 & h & 0 \\ h & 0 & 0 & 0 & -h \\ -h^2 & h^2 & 0 & h^2 & -h^2 \end{pmatrix}.$$

The difference scheme is then $\mathrm{Null}(N^{\mathrm{T}}) = [-1, -1, 4, -1, -1]$ (times an arbitrary constant), which coincides with the standard 5-point scheme for the Laplace equation. A more general case with different mesh sizes in the x- and y-directions is handled in a completely similar way.

The 3D case is also fully analogous. With six basis functions $\{1, x, y, z, x^2 - y^2, x^2 - z^2\}$ and the standard 7-point stencil on a uniform grid, one arrives, after computing the null space of the respective 6×7 matrix N^{T}, at the standard 7-point scheme with the coefficients $[-1, -1, -1, 6, -1, -1, -1]$. As in 2D, the case of different mesh sizes in the x-, y- and z-directions does not present any difficulty.

5.5. The fourth order 9-point Mehrstellen scheme for the Laplace equation in 2D

The solution is, by definition, a harmonic function. Harmonic polynomials are known to provide an excellent (in some sense, even optimal [6]) approximation of harmonic functions [1,6,13,75]. The following result is cited in [6]:

Theorem (Szegö). *Let $\Omega \subset R^2$ be a simply connected bounded Lipschitz domain. Let $\tilde{\Omega} \supset\supset \Omega$ and assume that $u \in L^2(\tilde{\Omega})$ is harmonic on $\tilde{\Omega}$. Then there is a sequence $(u_p)_{p=0}^{\infty}$ of harmonic polynomials of degree p such that*

$$\begin{aligned} \|u - u_p\|_{L^\infty(\Omega)} &\leqslant c \exp(-\gamma p) \|u\|_{L^2(\tilde{\Omega})}, \\ \|\nabla(u - u_p)\|_{L^\infty(\Omega)} &\leqslant c \exp(-\gamma p) \|u\|_{L^2(\tilde{\Omega})}, \end{aligned} \tag{59}$$

where γ, $c > 0$ depend only on Ω, $\tilde{\Omega}$.

For comparison, the H^1-norm error estimate in the standard FEM is

Theorem. [23,22,8] *For a family of quasi-uniform meshes with elements of order p and maximum diameter h, the approximation error in the corresponding finite element space V^n is*

$$\inf_{v \in V^n} \|u - v\|_{H^1(\Omega)} = C h^{\mu - 1} p^{-(k-1)} \|u\|_{H^k(\Omega)},$$

where $\mu = \min(p + 1, k)$ and c is a constant independent of h, p, and u.

For a fixed polynomial order p, the FEM and harmonic polynomial estimates are similar (factor $\mathrm{O}(h^p)$ vs. $\mathrm{O}([\exp(-\gamma)]^p)$ if the solution is sufficiently smooth. However, the FEM approximation is realized in a much wider space containing *all* polynomials up to order p, not just the harmonic ones. For solving the Laplace equation, the standard FE basis set can thus be viewed as having substantial redundancy that is eliminated by using the harmonic basis.

With these observations in mind, one may choose the basis functions as harmonic polynomials in x, y up to order 4, namely, $\{1, x, y, xy, x^2 - y^2, x(x^2 - 3y^2), y(3x^2 - y^2), (x^2 - y^2)xy, \ (x^2 - 2xy - y^2) \ (x^2 + 2xy - y^2)\}$. Then for a 3×3 stencil of adjacent nodes of a uniform Cartesian grid, the computation of the nodal matrix (16) (transposed) and its null space is simple with any symbolic algebra package. If the mesh size is equal in both x- and y-directions, the resultant scheme has order 6. Its coefficients are 20 for the central node, -4 for the four mid-edge nodes, and -1 for the four corner nodes of the stencil. In the standard texts [28,95], this scheme is developed by manipulating the Taylor expansions for the solution and its derivatives.

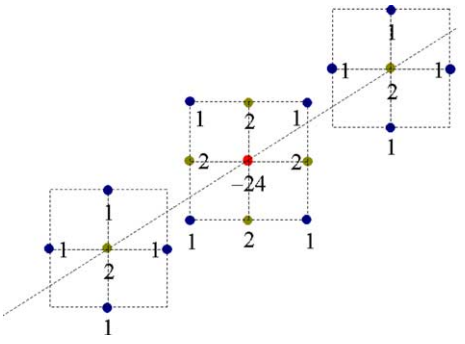

Fig. 6. For the Laplace equation, this 4th-order 'Mehrstellen'–Collatz scheme on the 19-point stencil is a direct particular case of Trefftz-FLAME.

5.6. The 4th order 19-point Mehrstellen scheme for the Laplace equation in 3D

Construction of the scheme is analogous to the 2D case. The 19-point stencil is obtained by considering a $3 \times 3 \times 3$ cluster of adjacent nodes and then discarding the eight corner nodes. The basis functions are chosen as the 25 independent harmonic polynomials in x, y, z up to order 4. Computation of the matrix of nodal values (16) and of the null space of its transpose is straightforward by symbolic algebra. The resultant difference scheme is shown in Fig. 6, where the 19 stencil nodes are split into three layers for clarity and the mesh size is assumed the same in all three directions. This 19-point 4th-order scheme is well known (it was introduced and called a 'Mehrstellen' scheme by Collatz [28]; see also [95]) but is typically derived from completely different considerations and viewed as a separate type of scheme.[7] We can now see, however, that in the Trefftz-FLAME framework Mehrstellen schemes and classic Taylor-based schemes for the Laplace equation stem from the same root – namely, the nullspace equation (29). The scheme is defined by the chosen stencil and a harmonic polynomial basis.

As a side note, the 19-point Mehrstellen scheme, due to its geometrically compact stencil, reduces processor communication in parallel solvers and therefore has gained popularity in computationally intensive applications of physical chemistry and quantum chemistry: electrostatic fields of multiple charges, the Poisson–Boltzmann equation in colloidal and protein simulation, and the Kohn–Sham equation of density functional theory [19].

5.7. The 1D Schrödinger equation. FLAME schemes by variation of parameters

This test problem is borrowed from the comparison study by Chen et al. [21] of several FD schemes for the boundary value (rather than eigenvalue) problem for the 1D Schrödinger equation over a given interval $[a, b]$.

$$-u'' + (V(x) - E)u = 0, \quad u(a) = u_a, \quad u(b) = u_b. \tag{60}$$

The specific numerical example is the fifth energy level of the harmonic oscillator, with $V(x) = x^2$ and $E = 11$ ($= 2 \times 5 + 1$). For testing and verification, boundary conditions are taken from the analytical solution, and as in [21] the interval $[a, b]$ is $[-2, 2]$. The exact solution is

$$u_{\text{exact}} = (15x - 20x^3 + 4x^5)\exp(-x^2/2). \tag{61}$$

[7] A generalization of the Mehrstellen schemes, known as the HODIE schemes [71], will not be considered here.

To construct a Trefftz-FLAME scheme for (60) on a stencil $[x_{i-1}, x_i, x_{i+1}]$ (where $x_{i\pm1} = x_i \pm h$), one would need to take two independent local solutions of the Schrödinger equation as the FLAME basis functions. The exact solution in our example is reserved exclusively for verification and error analysis. We shall construct Trefftz-FLAME scheme *pretending* that the theoretical solution is not known, as would be the case in general for an arbitrary potential $V(x)$.

Thus in lieu of the exact solutions the basis set will contain their approximations. There are at least two ways to construct such approximations. This subsection uses a perturbation technique that produces a 4th-order scheme. The next subsection employs the Taylor expansion that leads to 3-point schemes of arbitrarily high order.

At an arbitrary point x_0 let

$$V(x) = \kappa^2 + \delta V, \quad \text{where} \quad \kappa^2 \equiv V(x_0), \tag{62}$$

$$u(x) = u_0(x) + \delta u(x), \tag{63}$$

$$u_0(x) = c_+ \exp(\kappa x) + c_- \exp(-\kappa x) \quad \text{with arbitrary } c_+, c_-. \tag{64}$$

Substituting these expressions into the Schrödinger equation and ignoring the higher order term, one gets the perturbation equation

$$\delta u'' - \kappa^2 \delta u = \delta V u_0. \tag{65}$$

Solving this equation by variation of parameters, one obtains after some algebra

$$\begin{aligned} u(x) &= u_0(x) + \delta u(x) \\ &= u_0(x) + \frac{1}{2}\exp(\kappa x)\int_{x_0}^{x} u_0(\xi)\exp(-\kappa\xi)\delta V(\xi)\,\mathrm{d}\xi - \frac{1}{2}\exp(-\kappa x)\int_{x_0}^{x} u_0(\xi)\exp(\kappa\xi)\delta V(\xi)\,\mathrm{d}\xi. \end{aligned} \tag{66}$$

Two independent sets of values for c_+, c_- then yield two basis functions for FLAME.

Fig. 7 compares convergence of several schemes: the well-known Numerov scheme, the "Numerov–Mickens scheme" [21], Trefftz-FLAME, and the Mickens scheme [78,21]. The first three schemes are all of order four, but the FLAME errors are much smaller. In the following section, the FLAME error is further reduced, in many cases to machine precision.

5.8. Super-high-order FLAME schemes for the 1D Schrödinger equation

For sufficiently smooth potentials $V(x)$, as in our example of the harmonic oscillator, one can expand the potential and the solution into a Taylor series around the central stencil node x_i to obtain two local independent solutions with any desired order of accuracy. Consequently, the order of the FLAME scheme can also be arbitrarily high, even though the stencil still has only three points.

For the 20th-order scheme as an example, the roundoff level is reached for the uniform grid with just 10–15 nodes (Table 1). For a fixed grid size and varying order of the scheme, the error falls off very rapidly as the order is increased and quickly saturates at the roundoff level (Fig. 8).

5.9. A singular equation

Reddien and Schumaker [93] (RS) proposed a spline-based collocation method for 1D singular boundary value problems and use the following example:[8]

$$(x^{0.5}u')' - x^{0.5}u = 0, \quad 0 < x < 1, \quad u(0) = 1, \quad u(1) = 0. \tag{67}$$

[8] This example is as a result of my short communication with Larry L. Schumaker and Douglas N. Arnold.

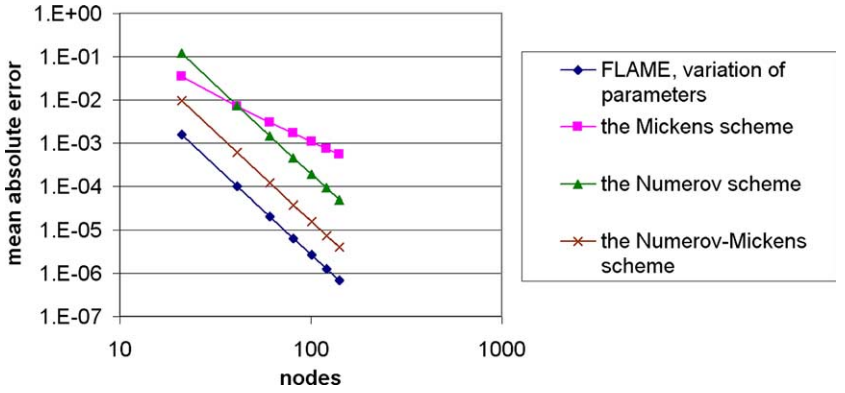

Fig. 7. Convergence of the variation of parameters – FLAME scheme for the Schrödinger equation. Comparison with other schemes described in [21] is very favorable (note the logarithmic scale). As the Numerov and Numerov–Mickens schemes, the FLAME scheme is of 4th-order but its error is much smaller. The Taylor version of FLAME (see below) performs much better still.

Table 1
Errors for the 3-point FLAME scheme of order 20

Number of nodes	Mean absolute error
7	2.14E−10
11	2.06E−14
15	1.75E−15

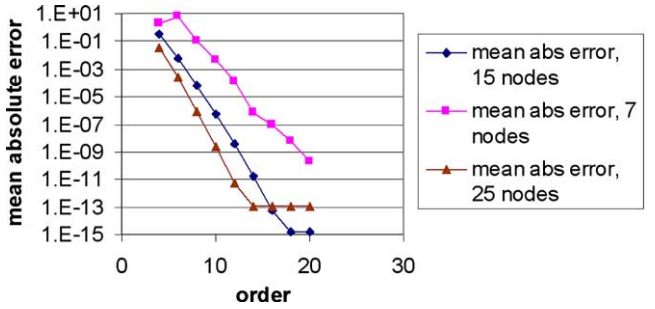

Fig. 8. Error vs. order of the Trefftz-FLAME scheme for the model Schrödinger equation.

Here we apply the nonvariational FLAME method to the same example and compare the results. A 3-point stencil on a uniform grid is used for FLAME. The two basis functions for FLAME are constructed separately for stencil points in the vicinity of the singularity point $x = 0$ and away from zero.

(1) Let the midpoint x_i of the ith stencil be sufficiently far away from zero (the singularity point of the differential equation): $x_i > \delta$, where δ is a chosen threshold. Expanding u over the ith stencil into the Taylor series with respect to $\xi = x - x_i$:

$$u = \sum_{k=0}^{\infty} c_k \xi^k \tag{68}$$

one obtains, by straightforward calculation, the following recursion:

$$c_{k+2} = \frac{c_k x_i + c_{k-1} - c_{k+1}(k+1)(k+\frac{1}{2})}{x_i(k+1)(k+2)}, \quad k = 0, 1, \ldots, \tag{69}$$

Table 2
Numerical values of the solution at $x = 0.5$: FLAME vs. other methods

n	FLAME, $K = 6$	FLAME, $K = 12$	RS [93]	Jamet [60]
8	0.25204513942296	0.252041978171219	0.25305	0.29038
16	0.252044597187729	0.252041977565477	0.25223	0.27826
8192	0.252042091673094	0.252041976551393		0.25310

The number of grid subdivisions and the order of the scheme in FLAME varied.

Table 3
Numerical errors of the solution at $x = 0.5$: FLAME vs. other methods.

n	FLAME, $K = 6$	FLAME, $K = 12$	RS [93]	Jamet [60]
8	3.16E−06	1.68E−09	1.01E−03	3.83E−02
16	2.62E−06	1.07E−09	1.88E−04	2.62E−02
8192	1.15E−07	5.80E−11		1.06E−03

The result for the FLAME scheme of order 40 with 8192 grid subdivisions was treated as 'exact' for the purposes of error evaluation.

where the coefficients with negative indices are understood to be zero. Two basis functions are obtained by choosing two independent sets of starting values for $c_{0,1}$ for the recursion and by retaining a finite number of terms, $k = K$, in series (68).

(2) For $x_i < \delta$, the approach is similar but the series expansion is different:

$$u = \sum_{k=0}^{\infty} b_k x^{k/2}. \tag{70}$$

Straightforward algebra again yields

$$\forall b_0, b_1; \quad b_2 = b_3 = 0,$$

$$b_{k+2} = \frac{4 b_{k-2}}{(k+1)(k+2)}, \quad k = 0, 1, \ldots \tag{71}$$

Two independent basis functions are then obtained in the same manner as above, with terms $k \leqslant 2K$ retained in (70).

Numerical values of the solution at $x = 0.5$ are given in [93,23] and serve as a basis for accuracy comparison. As Tables 2 and 3 shown below, Trefftz-FLAME gives orders of magnitude higher accuracy than the methods of [93,23]. The price for this accuracy gain is the analytical work needed for 'preprocessing', i.e. for deriving the FLAME basis functions.

This example is intended to serve as an illustration of the capabilities of FLAME and its possible applications; it does not imply that FLAME is necessarily better than all methods designed for singular equations. Many other effective techniques have been developed; see e.g. [67].

5.10. A summary of electromagnetic applications

Many electromagnetic applications of the Trefftz-FLAME schemes are described in [111]. These examples are briefly summarized here to provide a more complete picture of the existing applications of FLAME. In the following subsection a new simulation example of two coupled cylindrical nanoparticles is presented.

5.10.1. A line charge near a slanted boundary

This problem was chosen to illustrate how FLAME schemes can rectify the notorious 'staircase' effect that occurs when slanted or curved boundaries are rendered on Cartesian grids. The electrostatic field is generated by a line charge located near a slanted material interface boundary between air (relative dielectric

constant $\epsilon = 1$) and water ($\epsilon = 80$). This can be viewed as a drastically simplified 2D version of electrostatic problems in macro- and biomolecular simulation [98,94,46].

Four basis functions on a five-point stencil at the interface boundary were obtained by matching polynomial approximations in the two media via the boundary conditions. The Trefftz-FLAME result is substantially more accurate than solutions obtained with the standard flux-balance scheme and with the previously used variational version of FLAME.

5.10.2. A polarized elliptic particle

A dielectric cylinder, with an elliptic cross-section, is immersed in a uniform external field. An analytical solution [100] is imposed, for testing and verification purposes, as a Dirichlet condition on the exterior boundary of the domain. The usual 5-point stencil in 2D is used.

A nonstandard feature of the Trefftz-FLAME scheme in this problem is that, four basis functions being difficult to generate, only three were used. (The first basis function is simply equal to one, and the other two correspond to the analytical solutions for the external field applied in the x- and y-directions, respectively.) This arrangement produces a *two*-dimensional null space of the nodal matrix in FLAME. It then turns out to be possible to find a linear combination of the two independent difference schemes with a dominant diagonal entry, yielding a monotone difference operator.

5.10.3. Static fields of polarized or magnetized cylindrical particles (2D)

As a simple illustration of the efficiency of Trefftz-FLAME, compare two meshes (Fig. 9) that give about the same level of accuracy for a simple 2D test: a cylindrical magnetic particle with relative permeability $\mu = 100$ immersed in a uniform external field. An analytical solution for this problem is easily available and was imposed, for testing and verification purposes, as a Dirichlet condition on the domain boundary. The FE mesh has 125,665 degrees of freedom (d.o.f.); the relative error in the potential at the nodes is 2.07×10^{-8}. The FLAME grid has 900 d.o.f. (30×30), and the relative error in the potential at the nodes is 2.77×10^{-8} if 9-point (3×3) stencils are used.

5.10.4. Static fields of polarized or magnetized spherical particles (3D)

Problems of this type arise, in particular, in the simulation of colloidal systems [36,33]. Colloidal particles typically carry a surface electric charge giving rise to an electrostatic field. In some cases, particles can also be magnetic; controlling them by external magnetic fields may have interesting applications in some

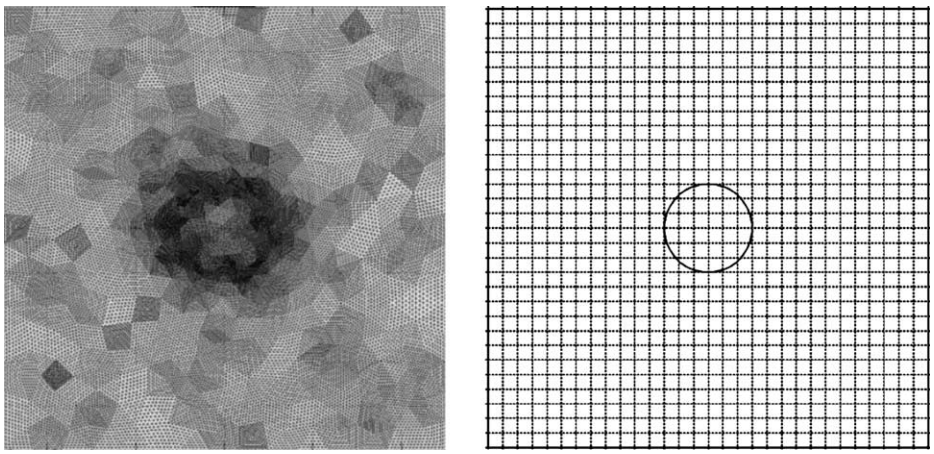

Fig. 9. Two meshes yielding about the same level of accuracy for the magnetic particle problem. The FE mesh has 31,537 nodes, 62,592 second order triangular elements and 125,665 degrees of freedom. The FLAME grid has 900 degrees of freedom.

emerging areas of nanoscale assembly [121,122,90]. Although the equation itself is simple, computationally the problem is quite challenging due to many-body interactions and the inhomogeneities.

In a solvent without salt (or in air) the electrostatic potential is governed by the Laplace equation both inside and outside the particles, with the standard conditions at particle boundaries.

For monovalent salts, the potential in the solvent can be described, with a good level of accuracy, by the Poisson–Boltzmann equation. (For multivalent salts, the correlation effects between the ions of the salt complicate the matter.)

In Trefftz-FLAME schemes, a 7-point stencil is used throughout the computational domain. In the vicinity of a particle, the local basis functions are obtained via spherical harmonics (which obviously have different forms for the Laplace and the linearized Poisson–Boltzmann equation). Away from particles, the standard 7-point scheme is employed.

5.10.5. Scattering from a dielectric cylinder

In this classic example, a monochromatic plane wave impinges on a dielectric circular cylinder and gets scattered. The analytical solution is available via cylindrical harmonics [54] and can be used for verification and error analysis. The basis functions in FLAME are cylindrical harmonics in the vicinity of the cylinder and plane waves away from the cylinder. The 9-point (3×3) stencil is used throughout the domain (with the obvious truncation to 6 and 4 nodes at the edges and corners, respectively). A new perfectly matched layer is introduced in some test cases [111]. Very rapid 6th-order convergence of the nodal values of the field was experimentally observed when the Dirichlet conditions were imposed on the exterior boundary of the computational domain. It would be quite difficult to construct a conventional difference scheme with comparable accuracy in the presence of such material interfaces.

5.10.6. Wave propagation in a photonic crystal

An interesting example was given by Fujisawa and Koshiba [43,117]. The waveguide with a bend is formed by eliminating a few dielectric cylindrical rods from a 2D array. This problem was solved by Trefftz-FLAME, with the same scheme as for the scattering problem above. Analysis of results and their convergence has shown that the Trefftz-FLAME simulation on a 50×50 Cartesian grid yields the same level of accuracy as a FEM simulation with 77,104 second order triangular elements (154,461 degrees of freedom).

5.11. Coupled plasmon nanoparticles

5.11.1. The plasmon resonance phenomenon

In the classic example of the electrostatic field distribution around a dielectric spherical particle immersed in a uniform external field, the potential can be easily found analytically via spherical harmonics. In fact, since the uniform field (say, in the z-direction) has only one harmonic component ($u = -E_0 z = -E_0 r\cos\theta$, in the usual notation), the solution also happens to contain only the dipole harmonic.

The field inside the particle can be expressed as [54,100]

$$E = E_0 \frac{3\epsilon_p}{\epsilon_p + 2\epsilon_{out}}, \tag{72}$$

where ϵ_p, ϵ_{out} are the dielectric constants of the particle and the surrounding medium, respectively. Other related physical quantities (the dipole moment, the polarizability, the field outside the particle) are expressed similarly and all share a singularity point at $\epsilon_p = -2\epsilon_{out}$.

Under normal electrostatic conditions, the singularity never manifests itself because the dielectric constants are all positive. However, in time-harmonic fields, the effective dielectric constant of materials generally becomes complex (reflecting the phase shift between the displacement vector **D** and the electric field **E**). For metals, at frequencies below the plasma frequency the effective permittivity happens to have a negative real part. This is of significant practical interest because the resonance condition (occurring at

$\epsilon_p = -2\epsilon_{out}$ for spheres, and at other negative values of ϵ_p for other shapes) can indeed be approached. These "plasmon" resonances of nanoparticles are becoming increasingly important in applications ranging from nanooptics to nanosensors to biolabels.

The high frequency case that gives rise to negative effective permittivities is, by definition, generally very far from electro*statics*. However, when the particle size is very small compared to the wavelength, the electrostatic approximation is reasonable, and a strong field enhancement is indeed possible. A true singularity, though, is never obtainable, for two reasons. First, the electrostatic treatment is precise only in the limit when the particle size tends to zero relative to the wavelength; for actual finite sizes of the particle the field enhancement is diminished due to dephasing effects. Secondly, and perhaps more importantly, the actual values of the dielectric constants are never purely real – the nonzero imaginary parts reflect the presence of losses in the material and blur the resonances.

Although the electrostatic approximation does provide a very useful insight, accurate evaluation of the resonance conditions and the field enhancement requires electromagnetic wave analysis. The governing equation for the H-mode (one-component H-field perpendicular to the computational plane and the electric field in the plane).

$$\nabla \cdot (\epsilon^{-1} \nabla H) + \omega^2 \mu H = 0. \tag{73}$$

The standard notation for frequency ω, permittivity ϵ and magnetic permeability μ is used. In the plasmon problem, the permeability can be assumed equal to μ_0 throughout the domain; the permittivity is ϵ_0 in air and has a complex and frequency-dependent value within plasmon particles. Any standard radiation boundary conditions for the scattered wave can be used.

Note that in the H-mode (but not in the complementary E-mode) the electric field "goes through" the plasmon particles, as it does in the electrostatic limit, thereby potentially giving rise to plasmon resonances.

As an illustrative example, the following subsections describe the construction of Trefftz-FLAME schemes for the problem proposed by Kottmann and Martin [65]. The physical setup involves two cylindrical plasmon particles with a small separation between them (Fig. 10) and leads to some interesting physical effects [65] (that are completely beyond the scope of this paper). Kottmann and Martin used integral equations in their simulation.

5.11.2. Trefftz-FLAME schemes away from the particles

We consider Trefftz-FLAME schemes on a 9-point (3×3) stencil. It is natural to choose the basis functions as cylindrical harmonics in the vicinity of each particle and as plane waves away from the particles. 'Vicinity' is defined by an adjustable threshold: $r \leqslant r_{cutoff}$, where r is the distance from the midpoint of the stencil to the center of the nearest particle, and the threshold r_{cutoff} is typically chosen as the radius of the particle plus a few grid layers.

Away from the particles, eight basis functions are taken as plane waves propagating toward the central node of the nine-point stencil from each of the other eight nodes:

$$\psi_\alpha = \exp(ik\hat{\mathbf{r}}_\alpha \cdot \mathbf{r}), \quad \alpha = 1, 2, \ldots, 8, \quad k^2 = \omega^2 \mu_0 \epsilon_0. \tag{74}$$

Here the origin of the coordinate system is placed at the midpoint of the stencil and $\hat{\mathbf{r}}_\alpha$ is the unit vector in the direction toward the respective node of the stencil, i.e.

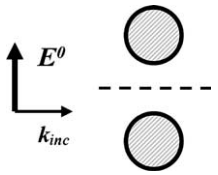

Fig. 10. Two cylindrical plasmon particles. Setup due to Kottmann and Martin [65].

$$\hat{\mathbf{r}}_\alpha = \hat{x}\cos\left(\alpha\frac{\pi}{4}\right) + \hat{y}\sin\left(\alpha\frac{\pi}{4}\right), \quad \alpha = 1,2,\ldots,8. \tag{75}$$

The 9×8 nodal matrix (16) of FLAME comprises the values of the chosen basis functions at the stencil nodes, i.e.

$$N_{\beta\alpha} = \psi_\alpha(\mathbf{r}_\beta) = \exp(\mathrm{i}k\hat{\mathbf{r}}_\alpha\cdot\mathbf{r}_\beta), \quad \alpha = 1,2,\ldots,8; \;\; \beta = 1,2,\ldots,9. \tag{76}$$

The Trefftz-FLAME scheme (29) is $\underline{s} = \mathrm{Null}(N^{\mathrm{T}})$. Straightforward symbolic algebra computation shows that this null space is indeed of dimension one, so that a single valid Trefftz-FLAME scheme exists. This scheme is defined up to an arbitrary factor and can be normalized in accordance with (41), with the right hand side f defined in (40).

To specify the normalization condition, it is sufficient to consider the wave equation (in air) with a constant right-hand side f_0 (viewed as a zero-order approximation of any smooth $f(x,y)$):

$$\nabla^2 H + k^2 H = f_0. \tag{77}$$

A particular solution of this equation is

$$H_f = \frac{f_0}{k^2}. \tag{78}$$

Then the right-hand side of the inhomogeneous Treffz-FLAME difference equation is

$$\underline{f}_{hi} = \underline{s}^{(i)\mathrm{T}}\mathcal{N}^{(i)}H_f = \frac{f_0}{k^2}\sum_{\beta=1}^{9} s_\beta, \tag{79}$$

where the fact that H_f is constant (78) was taken into account. Since the dependence of consistency and convergence parameters on k is not important here, the k^2 factor will be dropped from the normalization for convenience. The normalized scheme can then be constructed in two steps:

1. Pick $\tilde{s} \in \mathrm{Null}(N^{\mathrm{T}})$.
2. Normalize the scheme: $\underline{s} = \tilde{s}/\sum_{\beta=1}^{9}\tilde{s}_\beta$ (assuming that the sum is nonzero).

This normalization is as straightforward in symbolic algebra as the computation of the null space. The end result is given in the Appendix.

Substituting the nodal values of a 'test' plane wave $\exp(-\mathrm{i}k\hat{\mathbf{r}}\cdot\mathbf{r})$, where $\hat{\mathbf{r}} = \hat{x}\cos(\phi) + \hat{y}\sin(\phi)$, into the difference scheme, one obtains, after some more symbolic algebra manipulation, the consistency error

$$\epsilon_c = (hk)^6(\cos(\phi)-1)\cos^2(\phi)(\cos(\phi)+1)(2\cos^2(\phi)-1)^2/12,096, \tag{80}$$

where for simplicity the mesh size h is assumed to be the same in both coordinate directions.

The ϕ-dependent factor has its maximum of $(2-2^{\frac{1}{2}})/8$ at $\cos 2\phi = (\frac{1}{2}+2^{\frac{1}{2}}/4)^{\frac{1}{2}}$. Hence the consistency error $\epsilon_c \leqslant (hk)^6(2-2^{\frac{1}{2}})/96,768$. Since any solution of the Helmholtz equation in the air region can be locally represented as a superposition (Fourier integral) of plane waves, this result for the consistency error is in fact general. Note that by construction the scheme is exact for plane waves propagating in either of the eight special directions (at $\pm 45°$ to the axes if $h_x = h_y = h$).

Obviously, nodes at the domain boundary are treated differently. At the edges of the domain, the stencil is truncated in a natural way to six points: 'ghost' nodes outside the domain are eliminated, and the respective *incoming* plane waves associated with them are likewise eliminated from the basis set. The basis thus consists of five plane waves: three strictly outgoing and two sliding along the edge.

A similar procedure is applied at the corner nodes: a four-node stencil is obtained, and only three plane wave remain in the basis. The elimination of incoming waves from the basis thus leads to a FLAME-style PML. A detailed study of this and other versions of FLAME PML will be reported elsewhere.

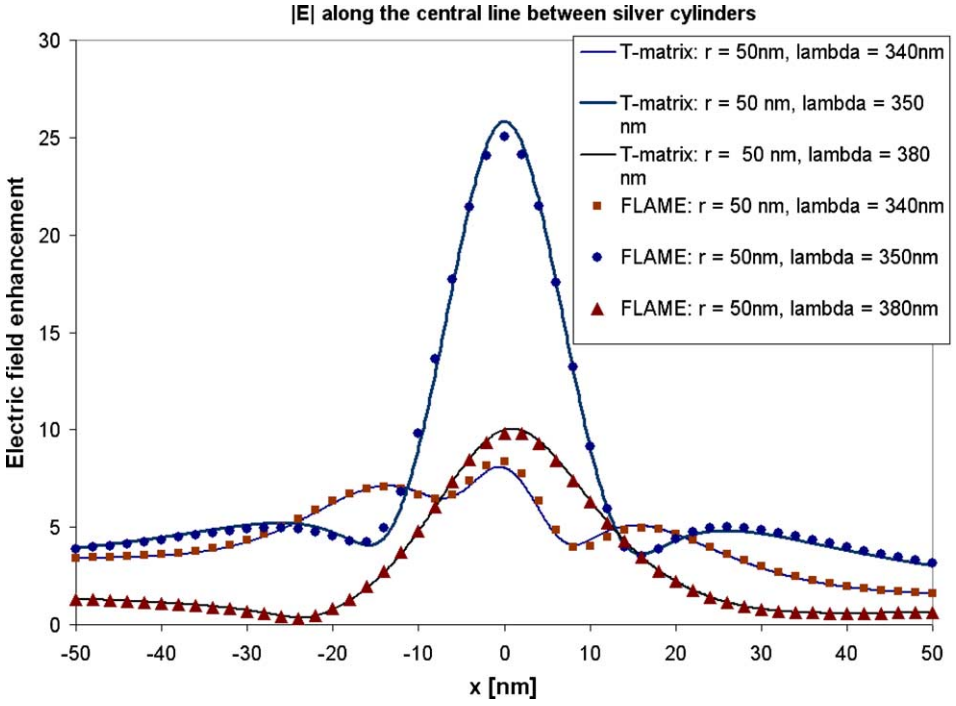

Fig. 11. The magnitude of the electric field along the line connecting two silver plasmon particles. Comparison of FLAME and multipole-multicenter results. Particle radii 50 nm; varying wavelength of incident light.

5.11.3. Trefftz-FLAME schemes in the vicinity of a particle

The 'Trefftz' basis functions satisfying the wave equation are chosen as cylindrical harmonics in the vicinity of each particle:

$$\psi_\alpha^{(i)} = a_n J_n(k_{\text{cyl}} r)\exp(\mathrm{i}n\phi), \quad r \leqslant r_0,$$
$$\psi_\alpha^{(i)} = [b_n J_n(k_{\text{air}} r) + H_n^{(2)}(k_{\text{air}} r)]\exp(\mathrm{i}n\phi), \quad r > r_0,$$

where J_n is the Bessel function, $H_n^{(2)}$ is the Hankel function of the second kind [54], and a_n, b_n are coefficients to be determined. These coefficients are found via the standard conditions on the particle boundary; the actual expressions for these coefficients are too lengthy to be worth reproducing here but are easily usable in computer codes.

Eight basis functions are obtained by retaining the monopole harmonic ($n = 0$), two harmonics of orders $n = 1, 2, 3$ (i.e. dipole, quadrupole and octupole), and one of harmonics of order $n = 4$. Numerical experiments for scattering from a *single* cylinder, where the analytical solution is available for comparison and verification, show convergence (not just consistency error!) of order six for this scheme [111].

5.11.4. Numerical results

The Trefftz-FLAME schemes described above were applied to the problem with two cylindrical particles (Fig. 10). In Fig. 11, the electric field computed with Trefftz-FLAME is compared with the quasi-analytical solution via the multicenter-multipole expansion of the wave [112,81],[9] for the following parameters. The

[9] The analytical expansion was implemented by Frantisek Čajko.

radius of each silver nanoparticle is 50 nm. The wavelength of the incident wave varies as labeled in the figure; the complex permittivity of silver at each wavelength is obtained by spline interpolation of values reported by Johnson and Christy [64]. As evident from the figure, the results of FLAME simulation are in excellent agreement with the quasi-analytical computation.

6. Discussion

The "flexible approximation" approach combines analytical and numerical tools: it integrates local analytical approximations of the solution into numerical schemes in a simple way. Existing applications and special cases of FLAME are listed in the following table and fall under two categories. The first one contains standard difference schemes revealed as direct particular cases of Trefftz-FLAME. The second category contains FLAME schemes that are substantially more accurate than their conventional counterparts, often with a higher rate of convergence for identical stencils. Practical implementation of Trefftz-FLAME schemes is substantially simpler than FEM matrix assembly and comparable with the implementation of conventional schemes (e.g. flux-balance schemes). A current summary of examples and applications of Trefftz-FLAME schemes is listed below.

Application	Basis functions used in FLAME	Stencil used in FLAME	Accuracy of FLAME schemes	Comparison with standard finite-difference schemes
Standard schemes for the 3D Laplace equation	Local harmonic polynomials	Depends on the order	2nd order for the 7-point stencil	Standard schemes are a simple particular case of FLAME
Mehrstellen scheme for the 3D Laplace equation	Harmonic polynomials in x, y, z up to order 4	19-point	4th order	The "Mehrstellen"-Collatz scheme revealed as a natural particular case of FLAME
1D Schrödinger equation	High-order Taylor approximations to the solution	3-point	Any desired order	The Numerov scheme is 4th order. 3-point schemes of order higher than 4 not available
1D heat conduction with variable material parameter	Independent local solutions of the heat equation	3-point	Exact (machine precision in practice)	So-called "homogeneous" schemes [95] are a particular case of FLAME.
Time-domain scalar wave equation (one spatial dimension)	Traveling waves (polynomials times sinusoids)	5-point	2nd order in the generic case	In the generic case, equivalent to central differences. Much higher accuracy if a dominant frequency is present

Application	Basis functions used in FLAME	Stencil used in FLAME	Accuracy of FLAME schemes	Comparison with standard finite-difference schemes
Slanted material interface boundary	Local polynomials satisfying interface matching conditions	7-point in 3D, 5-point in 2D	2nd order	Standard schemes, unlike FLAME, suffer form 'staircase' effects
Unbounded problems	Multipole harmonics outside the computational domain	7-point in 3D	See [52]	Standard finite-difference schemes not applicable to unbounded problems
Charged colloidal particles, no salt	Spherical harmonics (up to quadrupole)	7-point	2nd order	Much higher accuracy than the standard flux-balance scheme
Charged colloidal particles, mono-valent salt (Poisson-Boltzmann)	Spherical Bessel harmonics (up to quadrupole)	7-point	2nd order	Much higher accuracy than the standard scheme
Scattering from a dielectric cylinder (frequency domain)	Plane waves in air and cylindrical harmonics near scatterer	9-point	6th order	Much higher accuracy than the standard scheme
Perfectly Matched Layer (frequency domain)	Outgoing plane waves	9-point	Under investigation	
Wave propagation in a photonic crystal	Cylindrical harmonics	9-point	6th order	Much higher accuracy than the standard scheme and FEM with 2nd order triangular elements
Coupled plasmon particles	Plane waves in air and cylindrical harmonics near particles	9-point	6th order	Much higher accuracy than the standard scheme

It is worth noting that FLAME schemes do not have any hidden parameters to contrive better performance. The schemes are completely defined by the choice of the basis set and stencil; it is the approximating properties of the basis that have the greatest bearing on the numerical accuracy.

The collection of examples in the table above inspires further analysis and applications of FLAME. The table is in no way exhaustive – for example, boundary layers in eddy current problems and in semiconductor simulation (the Scharfetter–Gummel approximation [97,42]), varying material parameters in some protein models [46,116], corner singularities, etc., could be added to this list. Naturally, the author is hopeful that FLAME schemes will eventually find their use in these and other areas. Future challenges include:

development of a more comprehensive mathematical theory and convergence analysis, with insights into the 'best' choice of bases and stencils; robust postprocessing tools for field and force computation from the potential in FLAME; schemes in the time domain; schemes for *systems* of equations and for vector fields (for example, time-dependent Maxwell equations); and, on a more practical side, moving from testing and verification to large-scale simulations.

The method is most powerful when good local analytical approximations of the solution are available. For example, the advantage of the special field approximation in FLAME for a photonic crystal problem is crystal clear in [111]. Similarly, problems with magnetizable or polarizable particles admit an accurate representation of the field around the particles in terms of spherical harmonics, and the resultant FLAME schemes are substantially more accurate than the standard control volume method.

The Trefftz-FLAME schemes are not variational, which makes their construction quite simple and sidesteps the notorious bottleneck of computing numerical quadratures. At the same time, given that this method is nonvariational and especially non-Galerkin, one cannot rely on the well-established convergence theory so powerful, for example, in finite element analysis. For the time being, FLAME methods need to be considered on a case-by-case basis, with the existing convergence results (Section 4.5) and experimental evidence (Section 5) in mind. Furthermore, again because the method is non-Galerkin, the system matrix is in general not symmetric, even if the underlying continuous operator is self-adjoint. In many – but not all – cases, this shortcoming is well compensated for by the superior accuracy and rate of convergence (Section 5).

FLAME schemes described in the paper use nodal values as the primary degrees of freedom (d.o.f.). Other d.o.f. could certainly be used, for example edge circulations of the field. The matrix of edge circulations would then be introduced instead of the matrix of nodal values in the algorithm, and the notion of the stencil would be modified accordingly. In the FE context (edge elements), this choice of d.o.f. is known to have clear mathematical and physical advantages in various applications [14,57,72,107] and is therefore worth exploring in the FLAME framework as well.

At the suggestion of the anonymous reviewer, let us in closing discuss the potential use of FLAME schemes either as a general-purpose methodology for engineering applications or, alternatively, as a relatively narrow set of techniques for experts in computational methods.

One likely scenario is that the ideas presented in this paper will prove useful for further development of difference schemes in various areas. Such schemes can be eventually incorporated into existing FD software packages for use by many researchers and practitioners.

In the foreseeable future, FEM, due to its unrivaled generality and robustness, will remain king of engineering simulation software. However, FLAME schemes may successfully occupy the niches where FEM has serious weaknesses. One example is the simulation of electrostatic multiparticle interactions in colloidal systems, where FEM is impractical (and fast multipole methods may not be suitable due to nonlinearity and inhomogeneities). Although at present colloidal interactions can be considered as a 'niche application',[10] the rapid progress of nanotechnology, and in particular nanoscale assembly, could make this 'niche', and consequently the role of FLAME, much more prominent. Software for large-scale Trefftz-FLAME simulations of electrostatic interactions in colloidal suspensions is currently under development.[11]

Similar observations can be made (perhaps to a lesser extent) regarding the simulation of macromolecules, including proteins and polyelectrolytes, where electrostatic interactions of atoms in the presence of the solvent are extremely important but are still only part of an enormously complicated physical picture. Yet another example of a 'niche application' that could grow very rapidly in the future is wave propagation in photonic crystals.

Furthermore, the FLAME methodology will receive a boost if it is proven that accurate local *numerical* solutions can be used in lieu of the analytical ones to construct FLAME bases. This would significantly

[10] Colloidal scientists might disagree with that, though.
[11] Joint work with E. Ivanova, S. Voskoboynikov, and G. Friedman.

expand possible applications of FLAME. One could envision solving local "mini-FEM" problems (that are dramatically simpler in terms of mesh generation, matrix assembly and solvers than the global problem) to generate local FLAME bases. FLAME schemes will continue to operate on simple and relatively coarse Cartesian grids that do not necessarily have to resolve all geometric features of the problem. The system matrix would continue to be of relatively low dimension, with a simple structure.

Finally, any algorithm used in modern engineering practice has to be *adaptive*. It is way too early now to tell if robust adaptive procedures can be built on the FLAME basis. Notably, however, the "multilevel approximation" framework is a natural setup for a posteriori error indicators. Namely, the discrepancies between several local solutions coexisting on overlapping patches (see Section 3.3) may serve as a natural error gauge.

In addition to practical usage and to the potential of generating new difference schemes in various applications, there is also some intellectual merit in having a unified perspective on different families of FD techniques such as low- and high-order Taylor-based schemes, the Mehrstellen schemes, the 'exact' schemes, some special schemes for electromagnetic wave propagation, the "measured equation of invariance", and more. This unified perspective is achieved through systematic use of local approximation spaces *in the finite difference context*.

Acknowledgments

This line of research was inspired by my communication with Markus Clemens, Rolf Schuhmann and Thomas Weiland from Technische Universität Darmstadt in 2002. Another source of this research was my previous work with Alexander Plaks and Leonid Proekt on Generalized FEM. I thank Gary Friedman for many stimulating discussions and for the idea of Trefftz-FLAME methods for unbounded problems. Frantisek Čajko implemented the multipole-multicenter solutions for coupled dielectric scatterers. I thank Jon Webb for many references and comments, and Dmitry Golovaty for reading the manuscript and suggesting numerous improvements. Finally, I am grateful to the anonymous reviewers for their extensive and thorough reports and for numerous additional references.

Appendix. Coefficients of the 9-Point Trefftz-FLAME scheme for the wave equation in free space

The mesh size h is for simplicity assumed to be the same in both x- and y-directions. A 3×3 stencil is used. The eight Trefftz-FLAME basis functions are taken as plane waves in eight directions of propagation (toward the central node of the stencil from each of the other nodes). The following coefficients of the Trefftz-FLAME scheme (29) are then obtained.

For the central node:

$$s_1 = \frac{(e_{\frac{1}{2}}+1)(e_{\frac{1}{2}}e_1 + 2e_{\frac{1}{2}}e_0 - 4e_{-\frac{1}{2}}e_1 + e_{\frac{1}{2}} - 4e_{-\frac{1}{2}} + e_1 + 2e_0 + 1)}{(e_0-1)^2(e_{-\frac{1}{2}}-1)^4}$$

For the four mid-edge nodes:

$$s_{2-5} = -\frac{e_{\frac{3}{2}}e_0 - 2e_{\frac{1}{2}}e_1 + 2e_{\frac{1}{2}}e_0 - 2e_{\frac{1}{2}} + e_0}{(e_0-1)^2(e_{-\frac{1}{2}}-1)^4}$$

For the four corner nodes:

$$s_{6-9} = \frac{e_{-\frac{1}{2}}(2e_{\frac{1}{2}}e_0 - e_{-\frac{1}{2}}e_1 - 2e_{-\frac{1}{2}}e_0 - e_{-\frac{1}{2}} + 2e_0)}{(e_0-1)^2(e_{-\frac{1}{2}}-1)^4}$$

where $e_\gamma = \exp(2^\gamma \mathrm{i}hk), \gamma = -\frac{1}{2}, 0, \frac{1}{2}, 1, \frac{3}{2}$.

References

[1] V.V. Andrievskii, On approximation of functions by harmonic polynomials, Math. USSR-Izvestiya 51 (1) (1987) 1–13.
[2] D.N. Arnold, F. Brezzi, B. Cockburn, L.D. Marini, Unified analysis of discontinuous Galerkin methods for elliptic problems, SIAM J. Numer. Anal. 39 (5) (2002) 1749–1779.
[3] S.N. Atluri, S.P. Shen, The meshless local Petrov–Galerkin (MLPG) method: a simple and less-costly alternative to the finite element and boundary element methods, CMES – Comput. Model. Eng. Sci. 3 (1) (2002) 11–51.
[4] S.N. Atluri, T. Zhu, A new meshless local Petrov–Galerkin (MLPG) approach in computational mechanics, Comput. Mech. 22 (1998) 117–127.
[5] I. Babuška, G. Caloz, J.E. Osborn, Special finite-element methods for a class of 2nd-order elliptic problems with rough coefficients, SIAM J. Numer. Anal. 31 (4) (1994) 945–981.
[6] I. Babuška, J.M. Melenk, The partition of unity method, Int. J. Numer. Meth. Eng. 40 (4) (1997) 727–758.
[7] Ivo Babuška, Uday Banerjee, John E. Osborn, Survey of meshless and generalized finite element methods: a unified approach, Acta Numer. 12 (2003) 1–125.
[8] Ivo Babuška, Manil Suri, The p and h–p versions of the finite element method, basic principles and properties, SIAM Rev. 36 (1994) 578–632.
[9] N.A. Baker, D. Sept, J. Simpson, M.J. Holst, J.A. McCammon, Electrostatics of nanosystems: application to microtubules and the ribosome, PNAS 98 (18) (2001) 10037–10041.
[10] Achim Basermann, Igor Tsukerman, Parallel generalized finite element method for magnetic multiparticle problems, LNCS 3402 of Springer Series: Lecture Notes in Computational Science and Engineering, Springer, 2005, pp. 325–339.
[11] T. Belytschko, Y. Krongauz, D. Organ, M. Fleming, P. Krysl, Meshless methods: an overview and recent developments, Comput. Meth. Appl. Mech. Eng. 139 (1–4) (1996) 3–47.
[12] T. Belytschko, Y.Y. Lu, L. Gu, Element-free Galerkin methods, Int. J. Numer. Meth. Eng. 37 (1994) 229–256.
[13] Stefan Bergman, Approximation of harmonic functions of three variables by harmonic polynomials, Duke Math. J. 33 (2) (1966) 379–387.
[14] Alain Bossavit, Computational Electromagnetism: Variational Formulations, Complementarity, Edge Elements, Academic Press, San Diego, 1998.
[15] C.L. Bottasso, S. Micheletti, R. Sacco, The discontinuous Petrov–Galerkin method for elliptic problems, Comput. Meth. Appl. Mech. Eng. 191 (31) (2002) 3391–3409.
[16] John P. Boyd, Chebyshev and Fourier Spectral Methods, Dover Publications, 2001.
[17] S.C. Brenner, L.R. Scott, The Mathematical Theory of Finite Element Methods, Springer, New York, 2002.
[18] F. Brezzi, L.P. Franca, A. Russo, Further considerations on residual free bubbles for advective–diffusive equations, Comput. Meth. Appl. Mech. Eng. 166 (1998) 25–33.
[19] E.L. Briggs, D.J. Sullivan, J. Bernholc, Real-space multigrid-based approach to large-scale electronic structure calculations, Phys. Rev. B 54 (20) (1996) 14362–14375.
[20] P. Castillo, B. Cockburn, I. Perugia, D. Schöotzau, An a priori error analysis of the local discontinuous Galerkin method for elliptic problems, SIAM J. Numer. Anal. 38 (5) (2000) 1676–1706.
[21] Rongqing Chen, Zhizhan Xu, Lan Sun, Finite-difference scheme to solve Schrödinger equations, Phys. Rev. E 47 (5) (1993) 3799–3802.
[22] P.G. Ciarlet, The Finite Element Method for Elliptic Problems, North-Holland Pub. Co., Amsterdam, New York, 1980.
[23] P.G. Ciarlet, P.-A. Raviart, General Lagrange and Hermite interpolation in R^n with applications to finite element methods, Arch. Rational Mech. Anal. 46 (1972) 177–199.
[24] M. Clemens, T. Weiland, Magnetic field simulation using conformal FIT formulations, IEEE Trans. Magn. 38 (2) (2002) 389–392.
[25] B. Cockburn, G.E. Karniadakis, C.-W. Shu, The development of discontinuous Galerkin methodsLecture Notes in Comput. Sci. Eng., 11, Springer-Verlag, New York, 2000, pp. 3–50.
[26] James B. Cole, High accuracy solution of Maxwell's equations using nonstandard finite differences, Comput. Phys. 11 (3) (1997) 287–292.
[27] J.B. Cole, High-accuracy FDTD solution of the absorbing wave equation, and conducting Maxwell's equations based on a nonstandard finite-difference model, IEEE Trans. Antennas Propagation 52 (3) (2004) 725–729.
[28] Lothar Collatz, The Numerical Treatment of Differential Equations, Springer, New York, 1966.
[29] L. Cordes, B. Moran, Treatment of material discontinuity in the element-free Galerkin method, Comput. Meth. Appl. Mech. Eng. 139 (1996) 75–89.
[30] C.M. Cortis, R.A. Friesner, Numerical solution of the Poisson–Boltzmann equation using tetrahedral finite-element meshes, J. Comput. Chem. 18 (13) (1997) 1591–1608.
[31] M. Crouzeix, P.A. Raviart, Conforming and nonconforming finite element methods for solving the stationary Stokes equation, RAIRO Anal. Numer. 7 (R–3) (1973) 33–76, MR 49:8401.

[32] Suvranua De, Klaus-Jürgena Bathe, Towards an efficient meshless computational technique: the method of finite spheres, Eng. Comput. 18 (1–2) (2001) 170–192.
[33] Markus Deserno, Christian Holm, Sylvio May, Fraction of condensed counterions around a charged rod: comparison of Poisson–Boltzmann theory and computer simulations, Macromolecules 33 (2000) 199–205.
[34] S. Dey, R. Mittra, A conformal finite-difference time-domain technique for modeling cylindrical dielectric resonators, IEEE Trans. MTT 47 (9) (1999) 1737–1739.
[35] C.D. Dimitropoulos, Brian J. Edwards, Kyung-Sun Chae, Antony N. Beris, Efficient pseudospectral flow simulations in moderately complex geometries, J. Comput. Phys. 144 (1998) 517–549.
[36] J. Dobnikar, D. Haložan, M. Brumen, H.-H. von Grünberg, R. Rzehak, Poisson–Boltzmann Brownian dynamics of charged colloids in suspension, Comput. Phys. Commun. 159 (2004) 73–92.
[37] C. Duarte, J. Oden, h-p adaptive method using clouds, Comput. Meth. Appl. Mech. Eng. 139 (1996) 237–262.
[38] C.A. Duarte, I. Babuška, J.T. Oden, Generalized finite element methods for three-dimensional structural mechanics problems, Comput. Struct. 77 (2) (2000) 215–232.
[39] C. Farhat, I. Harari, L.P. Franca, The discontinuous enrichment method, Comput. Meth. Appl. Mech. Eng. 190 (2001) 6455–6479.
[40] G.J. Fix, S. Gulati, G.I. Wakoff, On the use of singular functions with finite elements approximations, J. Comput. Phys. 13 (1973) 209–228.
[41] F. Fogolari, G. Esposito, P. Viglino, H. Molinari, Molecular mechanics and dynamics of biomolecules using a solvent continuum model, J. Comput. Chem. 22 (15) (2001) 1830–1842.
[42] Gary Friedman, private communication, 2002–2005.
[43] T. Fujisawa, M. Koshiba, Time-domain beam propagation method for nonlinear optical propagation analysis and its application to photonic crystal circuits, J. Lightwave Technol. 22 (2) (2004) 684–691.
[44] M. Fushiki, Molecular dynamics simulations for charged colloidal dispersions, J. Chem. Phys. 97 (2) (1992) 6700–6713.
[45] G.K. Gothard, S.M. Rao, T.K. Sarkar, M. Salazar Palma, Finite element solution of open region electrostatic problems incorporating the measured equation of invariance, IEEE Microwave Guided Wave Lett. 5 (8) (1995) 252–254.
[46] J.A. Grant, B.T. Pickup, A. Nicholls, A smooth permittivity function for Poisson–Boltzmann solvation methods, J. Comput. Chem. 22 (6) (2001) 608–640, and references therein.
[47] M. Griebel, M.A. Schweitzer, A particle-partition of unity method for the solution of elliptic, parabolic and hyperbolic PDE, SIAM J. Sci. Comp. 22 (3) (2000) 853–890.
[48] M. Griebel, M.A. Schweitzer, A particle-partition of unity method-part II: efficient cover construction and reliable integration, SIAM J. Sci. Comp. 23 (5) (2002) 1655–1682.
[49] M. Griebel, M.A. Schweitzer, A particle-partition of unity method-part III: a multilevel solver, SIAM J. Sci. Comp. 24 (2) (2002) 377–409.
[50] G. Ronald Hadley, High-accuracy finite-difference equations for dielectric waveguide analysis I: uniform regions and dielectric interfaces, J. Lightwave Technol. 20 (7) (2002) 1210–1218.
[51] G. Ronald Hadley, High-accuracy finite-difference equations for dielectric waveguide analysis II: dielectric corners, J. Lightwave Technol. 20 (7) (2002) 1219–1231.
[52] D. Halverson, G. Friedman, I. Tsukerman, Local approximation matching for open boundary problems, IEEE Trans. Magn. 40 (4) (2004) 2152–2154.
[53] I. Harari, E. Turkel, Fourth order accurate finite difference methods for time-harmonic wave propagation, J. Comput. Phys. 119 (1995) 252–270.
[54] Roger F. Harrington, Time-Harmonic Electromagnetic Fields, Wiley-IEEE Press, 2001.
[55] J.H. Henderson, S.M. Rao, Electrostatic solution for three-dimensional arbitrarily shaped conducting bodies using finite element and measured equation of invariance, IEEE Trans. Antennas Propagation 46 (11) (1998) 1660–1664.
[56] I. Herrera, Trefftz method: a general theory, Numer. Meth. Partial Diff. Eq. 16 (2000) 561–580.
[57] R. Hiptmair, Discrete Hodge operators, Numer. Math. 90 (2001) 265–289.
[58] B. Honig, A. Nicholls, Classical electrostatics in biology and chemistry, Science 268 (5214) (1995) 1144–1149.
[59] T.J.R. Hughes, Multiscale phenomena: Green's functions, the Dirichlet-to-Neumann formulation, subgrid-scale models, bubbles and the origins of stabilized methods, Comput. Meth. Appl. Mech. Eng. 127 (1995) 387–401.
[60] Pierre Jamet, On the convergence of finite-difference approximations to one-dimensional singular boundary-value problems, Numer. Math. 14 (1970) 355–378.
[61] J. Jirousek, Basis for development of large finite elements locally satisfying all field equations, Comp. Meth. Appl. Mech. Eng. 14 (1978) 65–92.
[62] J. Jirousek, N. Leon, A powerful finite element for plate bending, Comp. Meth. Appl. Mech. Eng. 12 (1977) 77–96.
[63] J. Jirousek, A.P. Zielinski, Survey of Trefftz-type element formulations, Comput. Struct. 63 (1997) 225–242.
[64] P.B. Johnson, R.W. Christy, Optical constants of the noble metals, Phys. Rev. B 6 (12–15) (1972) 4370–4379.

[65] Jörg P. Kottmann, Olivier J.F. Martin, Retardation-induced plasmon resonances in coupled nanoparticles, Opt. Lett. 26 (2001) 1096–1098.
[66] Y. Krongauz, T. Belytschko, EFG approximation with discontinuous derivatives, Int. J. Numer. Meth. Eng. 41 (1998) 1215–1233.
[67] Manoj Kumar, A new finite difference method for a class of singular two-point boundary value problems, Appl. Math. Comput. 143 (2–3) (2003) 551–557.
[68] L.A. Lambe, R. Luczak, J.W. Nehrbass, A new finite difference method for the Helmholtz equation using symbolic computation, Int. J. Comput. Eng. Sci. 4 (1) (2003) 121–144.
[69] G.R. Liu, Mesh Free Methods: Moving Beyond the Finite Element Method, CRC Press, 2002, See Chapter 7 for Meshless Local Petrov–Galerkin method.
[70] W. Liu, S. Jun, Y. Zhang, Reproducing kernel particle methods, Int. J. Numer. Meth. Fluids 20 (1995) 1081–1106.
[71] R.E. Lynch, J.R. Rice, A high-order difference method for differential equations, Math. Comput. 34 (1980) 333–372.
[72] C. Mattiussi, An analysis of finite volume, finite element, and finite difference methods using some concepts from algebraic topology, J. Comput. Phys. 133 (2) (1997) 289–309.
[73] S.A. Meguid, Z.H. Zhu, A novel finite element for treating inhomogeneous solids, Int. J. Numer. Meth. Eng. 38 (1995) 1579–1592.
[74] K.K. Mei, R. Pous, Z. Chen, Y.W. Liu, M.D. Prouty, Measured equation of invariance: a new concept in field computation, IEEE Trans. Antennas Propagation 42 (1994) 320–327.
[75] J.M. Melenk, Operator adapted spectral element methods I: harmonic and generalized harmonic polynomials, Numer. Math. 84 (1999) 35–69.
[76] J.M. Melenk, I. Babuška, The partition of unity finite element method: basic theory and applications, Comput. Meth. Appl. Mech. Eng. 139 (1996) 289–314.
[77] J.M. Melenk, K. Gerdes, C. Schwab, Fully discrete hp-finite elements: fast quadrature, Comput. Meth. Appl. Mech. Eng. 190 (2001) 4339–4364.
[78] Ronald E. Mickens, Nonstandard Finite Difference Models of Differential Equations, World Scientific, Singapore; River Edge, N.J, 1994.
[79] R.E. Mickens (Ed.), Applications of Nonstandard Finite Difference Schemes, World Scientific, Singapore; River Edge, NJ, 2000.
[80] W.E. Milne, Numerical Solution of Differential Equations, Dover Publications, New York, 1970.
[81] M.I. Mishchenko, L.D. Travis, A.A. Lacis, Scattering, Absorption, and Emission of Light by Small Particles, Cambridge University Press, 2002.
[82] S. Moskow, V. Druskin, T. Habashy, P. Lee, S. Davydycheva, A finite difference scheme for elliptic equations with rough coefficients using a Cartesian grid nonconforming to interfaces, SIAM J. Numer. Anal. 36 (2) (1999) 442–464.
[83] E.H. Mund, A short survey on preconditioning techniques in spectral calculations, Appl. Numer. Math. 33 (2000) 61–70.
[84] J.W. Nehrbass, Advances in Finite Difference Methods for Electromagnetic Modeling. Ph.D. Thesis, Ohio State University, 1996.
[85] J.T. Oden, I. Babuška, C.E. Baumann, A discontinuous hp finite element method for diffusion problems, J. Comput. Phys. 146 (1998) 491–519.
[86] S.A. Orszag, Spectral methods for problems in complex geometries, J. Comput. Phys. 37 (1) (1980) 70–92.
[87] R. Pasquetti, F. Rapetti, Spectral element methods on triangles and quadrilaterals: comparisons and applications, J. Comput. Phys. 198 (2004) 349–362.
[88] S.V. Patankar, Numerical Heat Transfer and Fluid Flow, John Benjamins Publishing Co., 1980.
[89] Andrew F. Peterson, Scott L. Ray, Raj Mittra, Computational Methods for Electromagnetics, Oxford University Press, 1998.
[90] A. Plaks, I. Tsukerman, G. Friedman, B. Yellen, Generalized finite element method for magnetized nanoparticles, IEEE Trans. Magn. 39 (3) (2003) 1436–1439.
[91] L. Proekt, I. Tsukerman, Method of overlapping patches for electromagnetic computation, IEEE Trans. Magn. 38 (2) (2002) 741–744.
[92] G.D. Raithby, K.E. Torrance, Upstream weighted differencing schemes and their application to elliptic problems involving fluid flow, J. Comput. Fluids 2 (1974) 191–206.
[93] G.W. Reddien, L.L. Schumaker, On a collocation method for singular two-point boundary value problems, Numer. Math. 25 (1976) 427–432.
[94] W. Rocchia, E. Alexov, B. Honig, Extending the applicability of the nonlinear Poisson–Boltzmann equation: Multiple dielectric constants and multivalent ions, J. Phys. Chem. B 105 (28) (2001) 6507–6514.
[95] A.A. Samarskii, The Theory of Difference Schemes, M. Decker, New York, 2001.
[96] R. Schuhmann, T. Weiland, Recent advances in finite integration technique for high frequency applications, vol. 4 of Springer Series: Mathematics in Industry, 2004, pp. 46–57.
[97] S. Selberherr, Analysis and Simulation of Semiconductor Devices, Springer-Verlag, 1984.
[98] T. Simonson, Electrostatics and dynamics of proteins, Rep. Prog. Phys. 66 (5) (2003) 737–787, and references therein..

[99] I. Singer, E. Turkel, High order finite difference methods for the Helmholtz equation, Comput. Meth. Appl. Mech. Eng. 163 (1998) 343–358.
[100] W.B. Smythe, Static and Dynamic Electricity, John Benjamins Publishing Co, 1989.
[101] A.K. Soh, Z.F. Long, Development of two-dimensional elements with a central circular hole, Comput. Meth. Appl. Mech. Eng. 188 (2000) 431–440.
[102] D.B. Spalding, A novel finite-difference formulation for differential expressions involving both first and second derivatives, Int. J. Numer. Meth. Eng. 4 (1972) 551–559.
[103] G. Strang, Variational Crimes in the Finite Element Method, Academic Press, New York, 1972, pp. 689–710.
[104] J.C. Strikwerda, Finite Difference Schemes and Partial Differential Equations, Wadsworth & Brooks, Pacific Grove, CA, 1989.
[105] T. Strouboulis, I. Babuška, K.L. Copps, The design and analysis of the Generalized finite element method, Comput. Meth. Appl. Mech. Eng. 181 (1–3) (2000) 43–69.
[106] A. Taflove, S.C. Hagness, Computational Electrodynamics Method: The Finite-Difference Time-Domain, Artech House Publishers, 2000.
[107] E. Tonti, Finite formulation of electromagnetic field, IEEE Trans. Magn. 38 (2) (2002) 333–336.
[108] Igor Tsukerman, Efficient computation of long-range electromagnetic interactions without Fourier Transforms, IEEE Trans. Magn. 40 (4) (2004) 2158–2160.
[109] Igor Tsukerman, Flexible local approximation method for electro- and magnetostatics, IEEE Trans. Magn. 40 (2) (2004) 941–944.
[110] I. Tsukerman, Toward generalized finite element difference methods for electro- and magnetostatics, vol. 4 of Springer Series: Mathematics in Industry, 2004, pp. 58–77.
[111] I. Tsukerman, Electromagnetic applications of a new finite-difference calculus, IEEE Trans. Magn. 41 (7) (2005) 2206–2225.
[112] Victor Twersky, Multiple scattering of radiation by an arbitrary configuration of parallel cylinders, J. Acoust. Soc. Am. 24 (1952) 42–46.
[113] Richard S. Varga, Matrix Iterative Analysis, Springer, Berlin, New York, 2000.
[114] V.V. Voevodin, Iu.A. Kuznetsov, Matritsy i Vychisleniia, Nauka, Moskva, 1984 [in Russian].
[115] Z.J. Wang, A.J. Przekwas, Yen Liu, A FV-TD electromagnetic solver using adaptive cartesian grids, Comput. Phys. Commun. 148 (2002) 17–29.
[116] T. Washio, private communication, 2002–2003.
[117] J. Webb, private communication, 2004–2005.
[118] A. Wiegmann, K.P. Bube, The explicit-jump immersed interface method: finite difference methods for PDEs with piecewise smooth solutions, SIAM J. Numer. Anal. 37 (3) (2000) 827–862.
[119] K.S. Yee, Numerical solution of initial boundary value problems involving Maxwell's equations in isotropic media, IEEE Trans. Antennas Propagation AP-14 (3) (1966) 302–307.
[120] K.S. Yee, J.S. Chen, The finite-difference time-domain (FDTD) and the finite-volume time-domain (FVTD) methods in solving maxwell's equations, IEEE Trans. Antennas Propagation 45 (3) (1997) 354–363.
[121] B. Yellen, G. Friedman, Programmable assembly of heterogeneous colloidal particle arrays, Adv. Mater. 16 (2) (2004) 111–115.
[122] B.B. Yellen, G. Friedman, K.A. Barbee, Programmable self-aligning ferrofluid masks for lithographic applications, IEEE Trans Magn. 40 (4) (2004) 2994–2996.
[123] H. Yserentant, On the multilevel splitting of finite-element spaces, Numer. Math. 49 (4) (1986) 379–412.
[124] W. Yu, R. Mittra, A conformal finite difference time domain technique for modeling curved dielectric surfaces, IEEE Microwave Wireless Comp. Lett. 11 (2001) 25–27.
[125] I.A. Zagorodnov, R. Schuhmann, T. Weiland, A uniformly stable conformal FDTD-method in Cartesian grids, Int. J. Numer. Model. 16 (2003) 127–141.